JAXA Research and Development Report

SPICA Mid-infrared Instrument Calibration plan

YAMAGISHI Mitsuyoshi, YAMAMURA Issei, OYABU Shinki, OOTSUBO Takafumi,
WADA Takehiko, ISHIHARA Daisuke, NAKAGAWA Takao, KANEDA Hidehiro
and HIRAHARA Yasuhiro

February 2022

Japan Aerospace Exploration Agency

Contents

SPICA Mid-infrared Instrument Calibration plan

YAMAGISHI Mitsuyoshi[*1,*6], YAMAMURA Issei1[*1,†], OYABU Shinki[*2], OOTSUBO Takafumi[*3], WADA Takehiko[*1], ISHIHARA Daisuke[*1], NAKAGAWA Takao[*1], KANEDA Hidehiro[*4] and HIRAHARA Yasuhiro[*5]

Abstract

Preparatory works for the calibration of SPICA Mid-infrared Instrument (SMI) are reported. We focus on three calibration items, flux, wavelength, and geometrical distortion, and discuss requirements, strategies, and candidates of celestial objects to be used for the calibration. Information of previous and ongoing space infrared astronomical missions is compiled as a reference. We confirm that the standard stars for the flux calibration used in other missions are also applicable for SMI. We investigate objects for wavelength calibration, and conclude that both planetary nebulae and Be stars are needed. In addition, we discuss possible use of molecular lines in red-giant stars for the high-resolution mode. Globular clusters are only the objects that provide a sufficient number of position references for the correction of the geometrical distortion, but further investigation is needed to establish the correction method. The total amount of the observing time for the calibration of SPICA/SMI well fits the allocation plan of the observing time. Information and consideration made so far shall also be useful for future space infrared astronomical missions.

1 Purpose of this document

This document summarizes the calibration plan of SPICA Mid-infrared Instrument (SMI; Wada et al., 2020) onboard SPICA (Space Infrared Telescope for Cosmology and Astrophysics; Roelfsema et al., 2018). Calibration is essentially important for accurate measurements and scientific discussions, and is an important part of the development and operation of astronomical instruments. Design and characterization of the instrument should be done in close relation to how the instrument is calibrated in the laboratory during the development phase and using observation data taken in orbit. Since instruments for infrared astronomical observations are designed to achieve high sensitivity, and are operated in cryogenic temperature, opportunities for pre-flight calibration are limited, and the calibration process during in-orbit operation is crucial. The calibration plan thus should be established as early as possible, so that appropriate design and development of the instrument as well as preparation of the calibration objects can be done well in advance. As the first step of this activity, we discuss the calibration plan for SPICA/SMI by referring to the plans of previous missions. Candidates for calibration standards are investigated. This document is structured as follows. Section 2 overviews the specifications of SMI. Section 3 describes the requirements for calibration accuracy and the calibration plans to achieve them. Finally, section 4 discusses appropriate astronomical targets to be used in the calibration.

2 SMI

2.1 Overview

SPICA has been considered as the next-generation infrared satellite mission based on the heritage of IRAS (Infrared Astronomical Satellite; Neugebauer et al., 1984), ISO (Infrared Space Observatory; Kessler et al., 1996), AKARI (Murakami et al., 2007), Spitzer(Werner et al., 2004), WISE (Wide-field Infrared Survey Explorer; Wright et al., 2010), and Herschel (Pilbratt et al., 2010). It is equipped with a 2.5-meter telescope cooled down to 8 K. Three highly sensitive scientific instruments, SMI (SPICA Mid-infrared Instrument), SAFARI (SPICA Far-infrared Instrument), and B-BOP (Magnetic field explorer with BOlometric Polarimeter) cover wavelengths from 10 to $350\,\mu$m. The telescope and the instruments are cooled down to the cryogenic temperature by radiation cooling and the mechanical cryocoolers. SPICA's observation capability is superior to the previous missions, especially in spectroscopy, leading us to open new infrared astronomy.

SMI is an instrument dedicated to mid-IR spectroscopy and imaging in the wavelength range from 10 to 36 μm (Wada et al., 2020). SMI has three spectroscopic channels; Low-Resolution spectroscopy (LR), Medium-Resolution spectroscopy (MR), and High-Resolution spectroscopy (HR), as well as one imaging channel at $34\,\mu$m (CAM). SMI/LR is designed to perform a high-efficiency spectral mapping. A multi-slit prism spectrometer scans a wide field of view (FoV) of $\sim 10' \times 12'$ area with four slits of $10'$ in length so that each slit covers $10' \times 3'$. SMI/LR covers the wavelength range of 17–36 μm with the spectral resolution $R \sim 100$. The spectrometer is operated in a combination of a $10' \times 12'$ slit viewer camera (CAM) to determine the positions of the slits on the sky. SMI/MR is a grating spectrometer with a long slit of $1'$ in length. It provides a high line-sensitivity ($\sim 2 \times 10^{-20}$ W/m^2 in 1 hr, 5σ), and a moderately high spectral-resolution ($R =$1300–2300). SMI/HR is an immersion grating spectrometer with a very high line-sensitivity ($\sim 0.5 \times 10^{-20}$ W/m^2 in 1 hr, 5σ), and a high spectral resolution($R \sim 30,000$). SMI/MR and HR are operated to observe the same position of the sky simultaneously and are able to perform spectral mapping (or dithering) of a relatively small ($\sim 1' \times 1'$) area of the sky by slewing the telescope, as is called slow-scan operation.

2.2 Operation and Observation Modes

SMI has the following five operation modes: (1) Off, (2) Stand-by, (3) Calibration, (4) Observation, and (5) Annealing.

1. Off mode: No primary power is supplied to SMI.

2. Stand-by mode: SMI is switched on, but the detectors are in low-power mode; no output signal and a small amount of heat generation. This operation mode generates housekeeping data only. SMI is set to be this mode when one of the other instruments (SAFARI or B-BOP) executes observations.

3. Calibration mode: An internal calibration is performed by using the calibration lamps. SMI provides science and housekeeping data.

4. Observation mode: SMI performs observations and provides science and housekeeping data.

5. Annealing mode: SMI detectors are annealed by increasing the detector temperature for a specified duration to mitigate the effects of cosmic-ray hitting. Only housekeeping data are generated.

Three instruments onboard SPICA will be operated exclusively. A group of observations carried out by each instrument in a certain period is called a "campaign". Each SMI observation campaign typically lasts for 2–3 days. Each campaign consists of one annealing operation, dark current measurements (optional), multiple science observations, and calibration observations. The campaign starts with an annealing operation that takes 2–3 hours. If dark measurements are required for a special purpose, such as observations of faint diffuse sources, additional observations of a dark sky region will be performed. The measured dark current data will be applied to the science observation data taken in the same observation campaign in the data processing. In the beginning of each science observation, the detector performance is checked by operating the calibration lamps. The calibration observations, especially for the wavelength and the absolute flux calibrations, will be regularly performed to monitor the time variation of the instrument performance. Frequent calibration observations ($\gg$ once per campaign) will be performed in an early phase of the mission in order to confirm the stability of the instrument performance. Once the stability is established, the frequency may be reduced to ∼once per campaign. The stability of the instrument performance will be monitored by the response to the calibration lump and dark sky.

2.3 Astronomical Observation Template (AOT)

Three SMI observation-modes are defined as "Astronomical Observation Template (AOT)". All observations including those for calibration purpose will be executed by AOT.

2.3.1 SMI Stare-mode spectroscopy

This AOT is used for targeted spectroscopic observations of a point-like source with SMI/LR, MR, and HR. The longest exposure time per frame is 600 sec for all channels. When the telescope slewing finishes, check-out of each channel with a calibration lamp is performed. Then an exposure toward the target is executed. The exposure may be repeated with a small dithering on a slit until a total exposure time reaches the required value.

2.3.2 SMI/LR and /CAM slow-scan mapping spectroscopy

This AOT performs slit scanning spectroscopic observations with SMI/LR to produce a spectral map of a $10' \times 12'$ area (one field unit) and CAM to produce an imaging map. LR and CAM data are produced simultaneously. Typical scan speed is slower than $0.05''$/sec, which will result in 5% broadening of the Point Spread Function at $\lambda = 20\,\mu$m at 0.5 Hz sampling. A slow-scan mapping of $3'$ length with LR can complete the spectral mapping in the field of view of $10' \times 12'$. After one slow-scan mapping, a small maneuver to the next FoV is carried out to make a larger map.

2.3.3 SMI/MR and /HR slow-scan mapping spectroscopy

This AOT is applied for SMI/MR and /HR spectral mapping observations of extended targets. The spectral mapping is performed by a slow-scan of the telescope with a speed of $0.05''$/sec, which will result in 5% broadening of the Point Spread Function at $\lambda = 20\,\mu$m at 0.5 Hz sampling. The spectral resolution is also degraded accordingly by the same amount. A larger area map can be obtained by maneuvers with a step of $1'$.

3 SMI calibration

3.1 Requirements for calibration accuracy

The requirements for the calibration accuracy to enable SPICA to meet the core science objectives are defined in SPICA Science Requirements Document (SciRD; Tauber & SPICA Science Study Team, 2021).

3.1.1 Flux calibration

The requirement for the absolute flux calibration accuracy is better than 10 % of the absolute flux at any wavelengths covered by SMI. Relative flux calibration refers to the calibration across a spectrum. The measured flux at one wavelength relative to another wavelength should be accurate within 0.1% for LR, and 1% for MR and HR, respectively.

3.1.2 Wavelength calibration

The absolute wavelength calibration accuracy across the wavelength coverage shall be < 0.2% for LR, and 10% for MR and HR with respect to the spectral resolution element.

3.1.3 Astrometric calibration

The requirement for absolute pointing accuracy for SPICA is $0.4''$ (APE; absolute performance error). To achieve this accuracy the source position on the detector should be determined with an accuracy of $\sim 0.1''$ for the sources with sufficiently high signal-to-noise ratio (S/N). One problem to be solved in the astrometric calibration is the distortion of observed images due to optical aberration, which is a nonlinear relationship between the pixels on the detector and the positions on the sky. The distortion needs to be corrected with the accuracy of $\sim 0.1''$, corresponding to 0.15 pixel on the detector, otherwise they produce systematic positional errors depending on the locations on the detector.

3.2 Calibration Strategy

Calibration observations are performed throughout all SPICA mission phases. In the pre-launch phases, the instrument performance is evaluated in the laboratory at FPI (Focal Plane Instrument) and FPIA (Focal Plane Instrument Assembly) levels. The laboratory tests will provide an initial calibration parameters for SMI key components. Plans for the laboratory tests have not been established yet and are not discussed in this document. The in-orbit calibration items are described below. Various astronomical objects will be observed as the in-orbit calibration sources. Time variation (or stability)of the detector response will also be monitored by the calibration sources or the monitoring fields.

3.2.1 Flux calibration

The flux calibration is carried out by observing infrared standard stars. The achieved calibration accuracy depends on the quality of the infrared standard sources. New faint IR standard stars may need to be established to meet the calibration requirement in a lower flux range. A filter leakage is checked by comparing data of *blue* objects (e.g., stars) and *red* objects (e.g., Uranus and Neptune; note that the main belt asteroids are *blue* beyond $20\,\mu$m). Based on our experiences of AKARI/IRC and Spitzer/IRS, the absolute flux accuracy of 10% and the relative flux accuracy of 1% are achievable. In AKARI/IRC photometry, the absolute flux accuracy of < 6% is achieved by observing the IR standard stars in the ecliptic pole regions (Tanabé et al., 2008). As for the relative flux accuracy, Arimatsu et al. (2011) reported that the standard deviation of the flux measured the IR standard stars is ~ 1% at $\lambda = 15\,\mu$m. Spitzer/IRS Instrument Handbook ver. 5.0[1] (IRS Instrument Team & Science User Support Team, 2011) describes that the relative flux uncertainty is less than 0.1%. We expect that the relative flux accuracy can be obtained at a similar level.

3.2.2 Wavelength calibration

The wavelength calibration in orbit will be made by celestial sources showing spectral lines of known wavelengths. Possible candidates for the absolute wavelength calibration are Be stars and planetary nebulae (PNe). Spitzer/IRS Instrument Handbook ver. 5.0 describes that the accuracy of the wavelength calibration is better than < 0.16%. Therefore, the accuracy of 0.2% is achievable. The wavelength calibration of HR is more challenging because a spectrum consists of segments corresponding to each Echelle order, and a sufficient number of wavelength references are required for each segment. We consider to carry out a relative calibration within each segment. A possible reference for this relative calibration is atmospheric molecular lines in red-giant stars. Molecules such as H_2O, CO_2, HCN, and C_2H_2 are known to be abundant in these stars and show spectral lines in the HR wavelength range. Results of a simple simulation to examine the feasibility of this strategy are given in Appendix A.3.

---

[1] https://irsa.ipac.caltech.edu/data/SPITZER/docs/irs/irsinstrumenthandbook/

3.2.3 Astrometric calibration

There are three issues for the astrometric calibrations; (1) geometric distortion within a focal image, (2) alignment between detectors and the reference position of the focal-plane, and (3) absolute astrometry. Time variation should be considered if there are moving parts or temperature/mechanical variation. Item (1) will be discussed in this document (Section 3.3.3). (2) and (3) are somewhat coupled. By comparing the reference position which AOCS (Attitude and Orbit Control System) of the spacecraft assumes to point and the actual direction of FoV derived from the observed data will provide the alignment information and its time variation. The information shall be reflected to the AOCS as offsets. The pointing accuracy is improved as observations are accumulated. In any case, the distortion correction is a primarily important step in the astrometric calibration.

3.2.4 Flat-field and Dark current

The flat-field data and the detector dark current data are two major issues for the calibration especially in the imaging observations. Since SMI/CAM does not have a cold shutter, it is not possible to measure the dark current directly. The following method is instead considered to obtain the flat-field data or the detector sensitivity per pixel. In addition, the effect of dark current uncertainty is discussed.

We express the signal count of each pixel as

$$y_i = a_i I + b_i, \tag{1}$$

where y_i is the total count in the pixel i, I is the intensity of the sky in MJy/sr, a_i is the conversion factor of the pixel i in count/(MJy/sr), and b_i is a dark count in the pixel i. When we observe two regions where the sky intensities, I_H and I_L, are different from each other, we get two equations,

$$y_{iH} = a_i I_H + b_i, \tag{2}$$
$$y_{iL} = a_i I_L + b_i. \tag{3}$$

The difference of the two equations is given as

$$y_{iH} - y_{iL} = a_i(I_H - I_L). \tag{4}$$

Comparing them with the value at pixel $i = 1$ (as a reference pixel), we can get the relative flat-field as

$$\frac{a_i}{a_1} = \frac{y_{iH} - y_{iL}}{y_{1H} - y_{1L}}. \tag{5}$$

From equations 2 and 3, we have a relative dark map,

$$\frac{b_i}{b_1} = \frac{y_{iL}I_H - y_{iH}I_L}{y_{1L}I_H - y_{1H}I_L}. \tag{6}$$

The value b_i/b_1 depends on IL and IH. Based on AKARI data, Kondo et al. (2016) derived the absolute intensity of zodiacal light with an uncertainty of $\leq 5\%$ at the ecliptic poles and the ecliptic plane. The value b_i/b_1 is expected to have a similar uncertainty. Generally, the contribution of the dark current to the detector output is much smaller than the signals from the zodiacal light in MIR. Therefore, the uncertainty of b_i/b_1 is expected to be negligible in many cases except for deep observations of a very dark sky. These observations are repeated at the beginning of each observation campaign and occasionally if needed.

In addition to the above measurements, we can monitor the dark current performance using the masked areas that are not directly illuminated by the celestial light, although a stray light may still affect these areas.

3.3 Calibration source

3.3.1 Flux calibration

Stars with spectral types of A and K have been mainly used for flux calibration in many previous and ongoing missions (e.g., MSX, ISO, IRTS, Spitzer, AKARI, WISE, Herschel, and JWST).An All-Sky calibrator network has been constructed, with the primary standard Sirius (Cohen et al., 1999). SPICA will naturally follow this standard track. Asteroids are often used for flux calibration in the far-infrared wavelengths, but they are more science targets than the calibration standards in the mid-infrared wavelengths.

3.3.2   Wavelength calibration

Emission line sources (stars and compact PNe showing intense fine structure lines) with accurately known systemic velocities and expansion velocities of the stellar winds can be good references for the wavelength calibration. A spectrum of HR mode consists of a number of segments corresponding to every Echelle order. Ro-vibrational transition lines of molecules such as H_2O, CO_2, HCN and C_2H_2 observed in the red-giant stars are considered to be used for the relative wavelength calibration, as they provide a number of lines densely covering the HR's wavelength range. The absolute wavelength reference points may be given by the emission line stars.

3.3.3   Astrometric calibration

Among the three calibration items listed in Section 3.2.3, here we focus on point (1),the geometric distortion within a focal image, as the other two issues need information of the focal-plane configuration and the attitude control system of the spacecraft. For the distortion correction, clouds of stars with known positions (at least relatively within the FoV of the detector) are used as the reference. Possible candidates are stellar clusters. Suitable candidates for SPICA/SMI are discussed in Section 4.3.

3.4   Requirements for the calibration observations

3.4.1   Flux calibration

In order to obtain an absolute flux-calibrated spectrum of an observed target, we have to establish a response function $R(\lambda)$ [Jy / ADU or W m^{-2} λ^{-1} / ADU; ADU is arbitrary data unit for detector output] with an uncertainty σ_R better than the requirement. $R(\lambda)$ can be derived by

$$R(\lambda) = S_{\mathrm{model}}(\lambda)/S_{\mathrm{obs}}(\lambda), \tag{7}$$

where $S_{\mathrm{model}}(\lambda)$ is the model flux density of a standard star and $S_{\mathrm{obs}}(\lambda)$ is the observed signal in ADU. The corresponding uncertainties are given as σ_{model} and σ_{obs}, respectively.

First, we estimate the number of independent stars required for the calibration. Let σ_{model} be typically 5% (e.g., Bohlin & Cohen, 2008) and random. We assume $\sigma_{\mathrm{model}} \gg \sigma_{\mathrm{obs}}$, hence σ_R is dominated by σ_{model}. The uncertainty of the averaged response function, $\overline{R(\lambda)}$, is given by

$$\overline{\sigma_R} = \sigma_R/\sqrt{n_{\mathrm{star}}}, \tag{8}$$

where n_{star} is the number of independent standard stars used for the calibration. To assure that $\overline{R(\lambda)}$ represents the 'real' value within an error of 1 %, n_{star} should be 25 or more.

Next, we consider the number of observations for each standard star needed to realize the above assumption, $\sigma_{\mathrm{model}} \gg \sigma_{\mathrm{obs}}$. The uncertainty of the averaged spectrum from n_{obs} observations, $\overline{S_{\mathrm{obs}}}$, is given by

$$\overline{\sigma_{\mathrm{obs}}} = \sigma_{\mathrm{obs}}/\sqrt{n_{\mathrm{obs}}}, \tag{9}$$

where n_{obs} is the number of observations repeated for a star. The standard stars will be chosen to be bright enough to achieve S/N > 100 for each observation. However, from our experiences (see Section A.2, Tabless 8, 9, and 10), effects from other factors (especially pointing stability in case of slit spectroscopy) would degrade the repeatability of $\sigma_{\mathrm{obs}}(\lambda)$. From Table 8, 9, and 10, it is reasonable to adopt $\sigma_{\mathrm{obs}} = 5$ %. To achieve $\overline{\sigma_{\mathrm{obs}}}$ to be 1 % (S/N = 100 and 1/5 of σ_{model}), n_{obs} should be 25 or more.

In total, 25×25 = 625 observations are requested for each spectroscopic observing mode. For the CAM mode, n_{obs} can be much less as it does not have a slit. We allocate 4 observations per star, i.e., 4×25 = 100 observations are requested for CAM.

3.4.2   Wavelength calibration

We expect that the spectrometer is stable enough along the wavelength dimension and that the wavelengths of reference lines are accurately known. Hence, only a few measurements are sufficient to complete the wavelength calibration. The requirement for source selection is that at least one source is available at any time during the mission, especially in the initial phase. Visibility is more important than the number of stars.

An estimate of the number of observations is made as follows. The standard stars are selected to be bright enough to provide a high S/N ratio for the measurement of line positions. LR and MR have long slits, and variation along

the slit needs to be considered. This will be made by a mapping mode observation. For LR, 9 points along a slit $\times 4$ slits = 36 data points will be measured. For MR, 3 points along the slit will be measured.

Calibration standards for HR have not been established so far. Red-giant stars are considered in this study. There are many bright red-giant stars in the sky, but further investigations are needed to create a concrete list of the objects. Since such stars are often variables of Mira type or Semi-regular type, we may have to observe multiple objects to find at least one appropriate spectrum. We also have to repeat the observations several times during the operation phase as spectra suitable for the calibration may be obtained from different stars time by time.

Although we expect that the instrument and the calibrators are stable over the operation period, we will periodically repeat the observations to monitor the repeatability and/or possible time variation. We suggest to observe at least one object per month for each channel, although a detailed investigation is needed. Thus, the number of observations is estimated to be 40 for the initial calibration and 54 months $\times 3$ channels = 162 for monitoring. In total ~ 200 observations are required in 4.5 years of science operation.

3.4.3 Distortion correction

An order estimate of the data points needed for the distortion correction of SMI/CAM is attempted. We set $9\times9 = 81$ positions on the sky, and calculate corresponding pixel positions on the detector by a ray-tracing simulation for the latest optical layout. We randomly mask a part of the 81 data points and reconstruct the position of these masked points from the remaining data points. Three collection methods are examined.

(1) **Empirical method:** Difference between the ideal (without distortion) position (x_0, y_0) and the observed (with distortion) position (x, y), $(dx, dy) = (x - x_0, y - y_0)$ is expressed by empirical functions of the observed position as $dx = f(x, y)$, $dy = g(x, y)$, where $f(x, y)$ and $g(x, y)$ are given by interpolation. We apply three algorithms (nearest, linear, and cubic) using Python scipy package, and find that the cubic interpolation is the best algorithm. We mask randomly-selected 8 data points (10% of the entire sample) and estimate these position from the remaining data points. The calculations are repeated 100 times and the average residual ($dr = \sqrt{(x_c - x_0)^2 + (y_c - y_0)^2}$, where (x_c, y_c) is the corrected position) is evaluated.

(2) **Inverse matrix method:** Holtzman et al. (1995) described a focal-plane distortion correction for HST/WFPC2. They expressed the observed (distorted) position of i-th pixel (x_i', y_i') by n_{th} order polynomial function (in their case cubic) of (x_i, y_i) as,

$$
\begin{aligned}
x_i' &= a_{00} \\
&+ a_{10}x_i + a_{20}x_i^2 + \cdots + a_{n0}x_i^n \\
&+ a_{01}y_i + a_{02}y_i^2 + \cdots + a_{0n}y_i^n \\
&+ a_{11}x_iy_i + a_{21}x_i^2y_i + \cdots + a_{n1}x_i^ny_i \\
&+ \cdots + a_{nn}x_i^ny_i^n,
\end{aligned}
\tag{10}
$$

Same as for y dimension. This can be summarized in a matrix form as,

$$
\begin{pmatrix}
x_1' \\
x_2' \\
x_3' \\
\vdots \\
x_n'
\end{pmatrix}
=
\begin{pmatrix}
1 & x_1 & y_1 & x_1^2y_1 & x_1y_1^2 & \cdots & x_1^ny_1^n \\
1 & x_2 & y_2 & x_2^2y_2 & x_2y_2^2 & \cdots & x_2^ny_2^n \\
1 & x_3 & y_3 & x_3^2y_3 & x_3y_3^2 & \cdots & x_3^ny_3^n \\
\vdots & \vdots & \vdots & \vdots & \vdots & \vdots & \\
1 & x_m & y_m & x_m^2y_m & x_my_m^2 & \cdots & x_m^ny_m^n
\end{pmatrix}
\begin{pmatrix}
a_{00} \\
a_{10} \\
a_{01} \\
\vdots \\
a_{nn}
\end{pmatrix}.
\tag{11}
$$

Once $(a_{00}, a_{10}, a_{01}, \cdots, a_{nn})$ is determined, the ideal position (x_i, y_i) can be calculated by the inverse matrix method. As the first approach we set 0 for the cross-terms and apply 2–4 order polynomial functions. We mask 4–8 points randomly selected from the 81 data points, and test how well we can reproduce these masked positions (distorted position) from the rest of the data points. We repeat the process 10,000-times, and the average of the residual between the estimated position and those from the ray-tracing is evaluated.

(3) **Inverse matrix method using IRAF/geomap:** A similar approach as (2) is adopted by using IRAF module `geomap` package with 4-th polynomial functions including the cross-terms.

The results are summarized in Table 1 and Figures 1 and 2. Our temporary conclusion from the analysis above is the following.

- The empirical method of polynomial interpolation of the distortion may work well for the complex geometry of the focal-plane, if a sufficient number of reference points are given.

- Polynomial expression of the distortion for the inverse matrix method (method (2) and (3)) do generally not work well for the SMI optics. Inclusion of the cross-terms (method (3)) would improve the results but still far from the requirement (0.15 pix). A reason is that the focal-plane geometry of the SMI is much more complex than a simple cubic polynomial function that can be adopted for HST/WFC2, because of the free-form-mirror-based design.

- The number of data points in the current analyses, 81, is too small to achieve the required correction accuracy. Analysis with larger data sample (at least 10 times more data points) should be done.

Since SMI/CAM and /LR has no moving parts such as the filter wheel, we expect that the distortion pattern is rather stable over the operation period. Only a possible factor that changes the distortion is the temperature of the system, though it should also be stable. In real flight operation, objects with high source density (see, Section 4.3) will be observed for distortion correction. Not so many objects and observations are expected to cover the SMI/CAM and /LR FoV.

Table 1: Results of distortion correction with 81 sample points.

Method	Residual (pix)	Note
(1)	2.1	Figure 1
(2) Order=2	8.6	Figure 2
(2) Order=3	4.2	Figure 2
(2) Order=4	3.8	Figure 2
(3) Order=4	1.5	

3.4.4 Estimate of SPICA/SMI calibration time

In summary, the number of calibration observations for SMI is $625 \times 3 + 100 + 200 \sim 2,200$. Assuming that each observation takes 30 minutes (mostly spacecraft overheads such as slewing and stabilization), the total observing time for calibration is 0.5 hours $\times$ 2,200 observations $\sim 1,100$ hours. Other calibration measurements, for instance the distortion correction, flat-fielding and calibration for diffuse sources are expected to be as much as a few hundred hours. SPICA's science operation lasts for 4.5 years $= \sim 40,000$ hours. If 10% of the total observing time (4,000 hours) is allocated to the calibration, SMI shares about 1/3 of the time.

Calibration time in previous space infrared astronomical missions are summarized in Appendix A.2 for comparison. It is found that the fraction of the calibration time to the total observing time in SPICA/SMI is comparable to the previous missions.
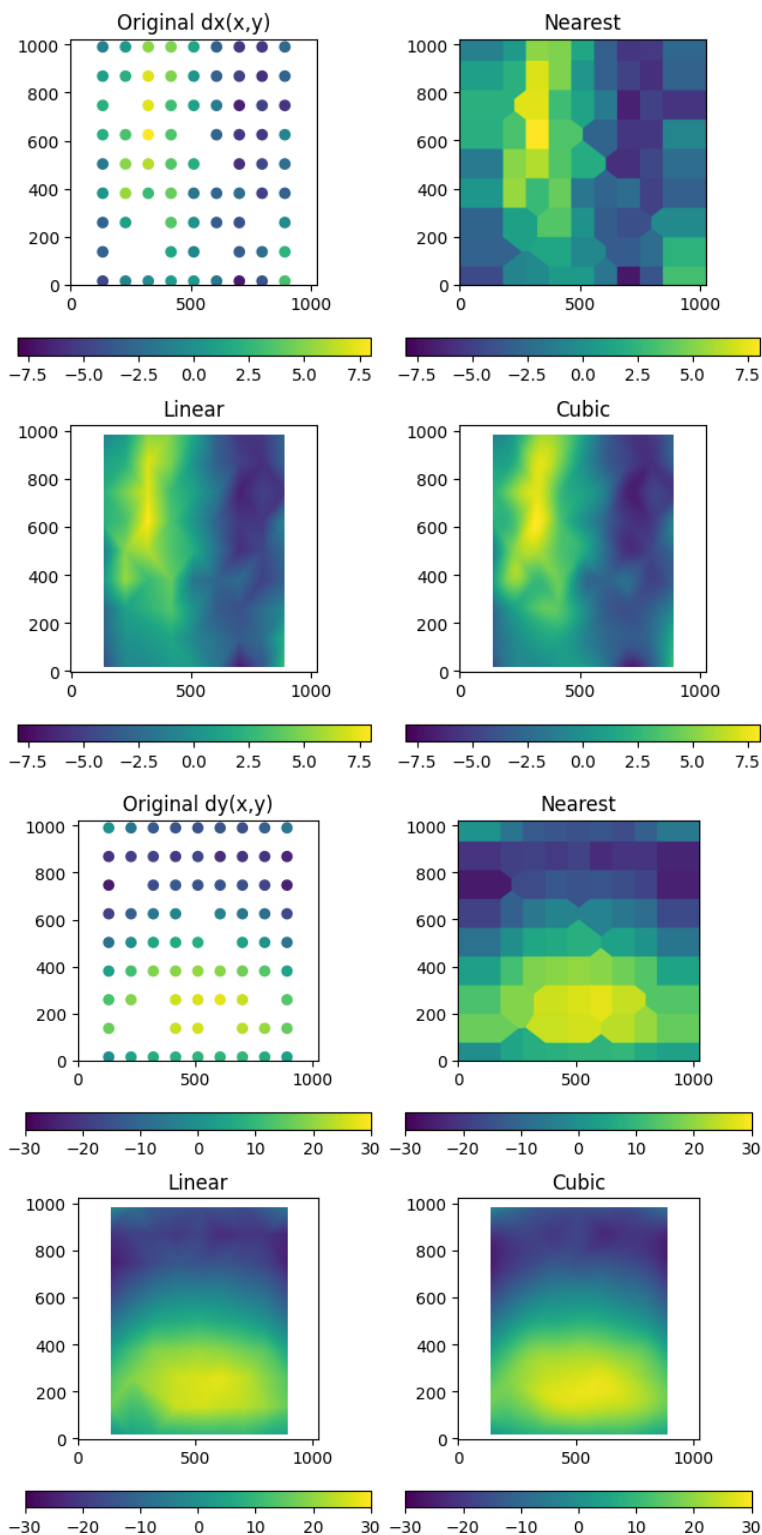
Figure 1: An example of the distortion correction using three interpolation algorithms. Color shows offset in x (top four panels) or y direction (bottom four panels) (i.e., $x - x_0$ or $y - y_0$) in unit of pixel from the position without distortion.
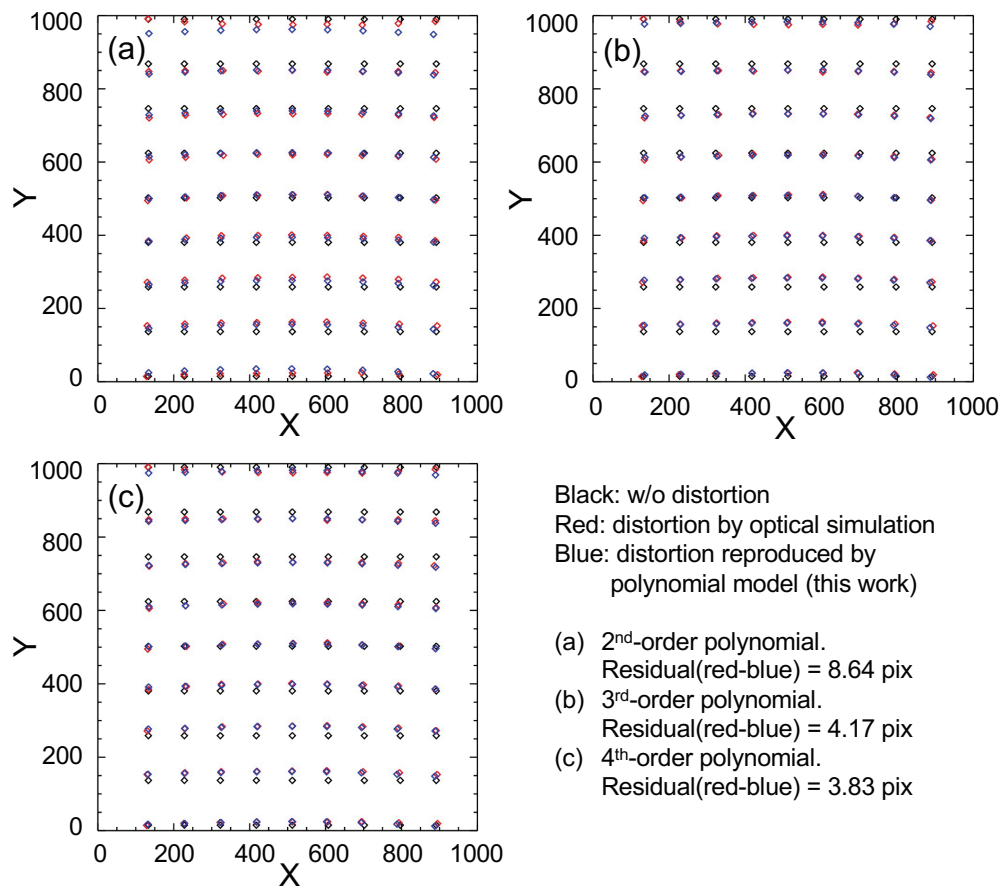
Figure 2: Distortion correction using the inverse matrix method. Black, red, and blue points are those without distortion, with distortion, and estimated position by the inverse matrix method (see text). Average residuals from 10,000-repeated tests are indicated in the right-bottom corner.

4 Target selection

4.1 Flux calibration

The suitable flux range of the calibration sources is evaluated for the target selection. We use SMI Time Estimator version 3.2 with the following input parameters.

- S/N = 100 for continuum level in the wavelength range of each channel in observation time (including overhead) < 30 minutes.

- Background level = 0 (Low background for extragalactic observations)

- Mapping area: $10' \times 1' \times 4$ (LR), $1' \times 1'$ (MR), $4'' \times 4''$ (HR), and $10' \times 12'$ (CAM).

Figure 3 summarizes the resultant observation time including overheads as a function of target flux. The flux ranges suitable for the calibration sources are estimated as 14 mJy–20 Jy at 27 μm (LR), 150 mJy–800 Jy at 27 μm (MR), 60 mJy–10000 Jy at 15 μm (HR), and 0.4 mJy–0.8 Jy at 34 μm (CAM). The upper side of each flux range is determined by the saturation limit of each channel.
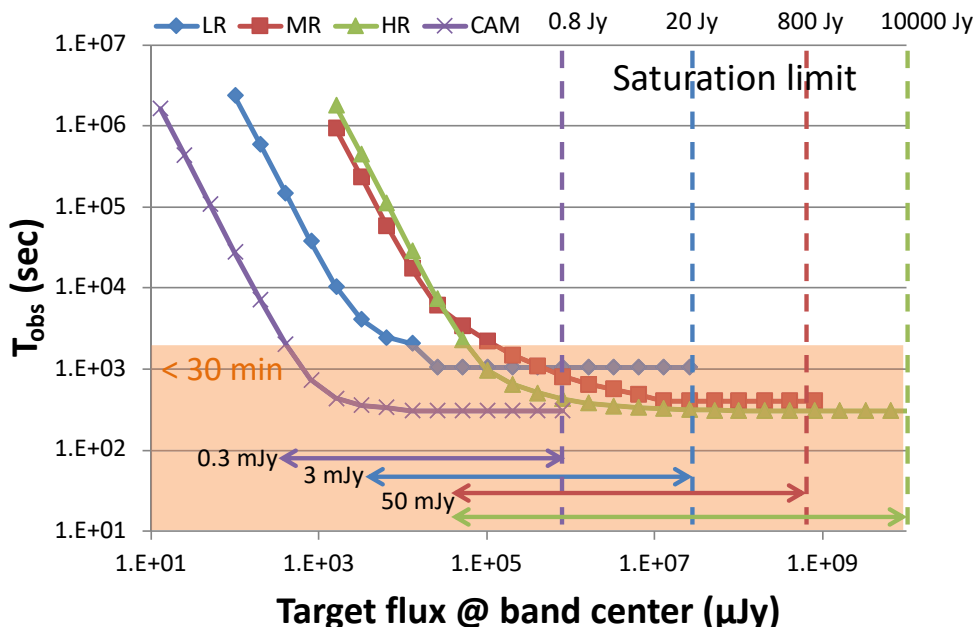
Figure 3: Observation time including overheads as a function of target flux.

It is found that the flux range suitable for the SMI flux calibration (Figure 3) can be covered by the targets prepared for Spitzer, AKARI, and JWST.

4.2 Wavelength calibration

The wavelength calibration is performed by comparing the wavelengths of emission (or absorption) lines and their pixel position on the detector arrays. The calibration sources must have sufficient spectral lines within the wavelength range of each channel. Here we examine two kinds of objects, planetary nebulae (PNe) and Be stars. The selection of calibrators described below is for LR and MR, which have similar wavelength coverage. Wavelength calibrators for HR are under investigation, as the spectral data of this mode consist of many fragments each of which covers a small wavelength range, and the calibration sources should usually have at least four wavelength references in each segment. Emission lines from PNe or Be stars are not dense enough to cover every order of the HR spectra. Molecular lines of H_2O, CO_2, HCN, and C_2H_2 are present in this wavelength range. A result of the initial assessment of using molecular lines for the wavelength calibration is explained in Appendix A.3.

4.2.1　PNe vs. Be stars

AKARI and Spitzer used PNe for the wavelength calibration, while JWST will use Be stars. We consider that both PNe and/or Be stars can be good wavelength calibrators for SMI. Since the wavelength ranges of LR and MR are almost identical, we consider MR only. Figure 4 shows examples of spectra of a planetary nebula and a Be star. In general, PNe show intense emission lines and weak continuum emission, while Be stars show relatively weak emission lines and intense continuum emission. Therefore, in terms of line detection, PNe are better than Be stars.

　MR covers its wavelength range by using six spectral orders (m=6–11). Each order needs to have multiple lines for proper calibration. Table 2 shows a list of expected emission lines from PNe and Be stars par spectral order. Both types of objects show multiple emission lines in the range of each order, except for order m=11 in which only one strong line is expected. It should be noted that the emission lines from PNe have a variety of ionization energy, indicating that not all of the lines are emitted from a single object. Therefore, to detect all the lines in the list, we need to observe multiple objects. On the other hand, all the lines from Be stars are hydrogen recombination lines, indicating that all the lines are observed simultaneously if a proper object is chosen. Hence, in terms of wavelength coverage of the emission lines, Be stars are better than PNe. Considering the above merits and demerits, we conclude that both PNe and Be stars are necessary for the wavelength calibration of SMI.
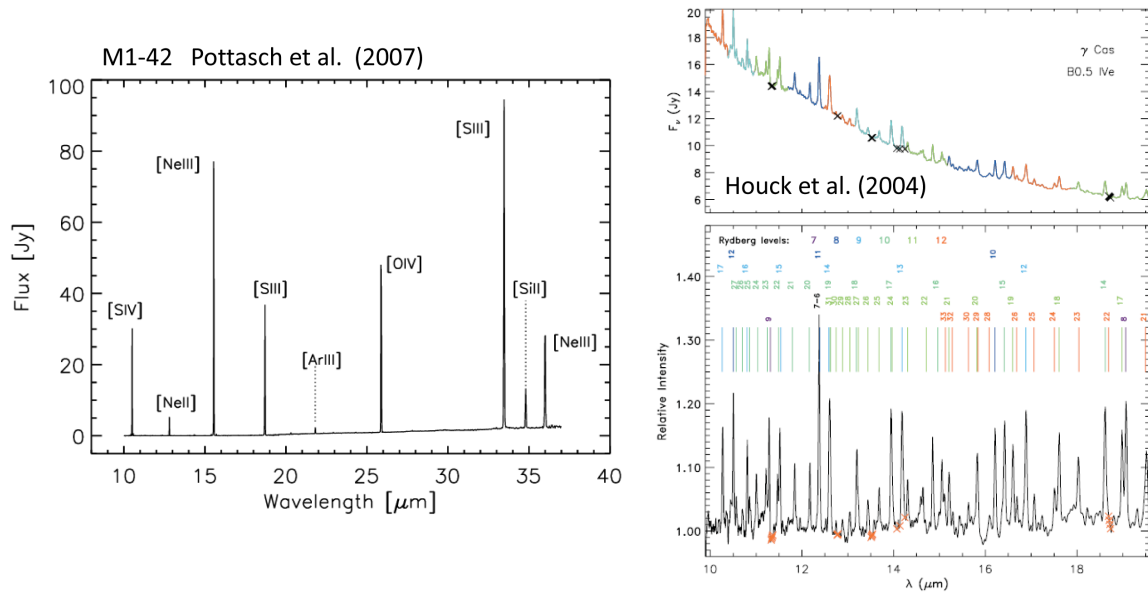
Figure 4: Example of spectra of a PN and a Be star (Pottasch et al., 2007; Houck et al., 2004) Reproduced by permission of the AAS.

4.2.2　PN candidates

We search for PN observation data in the Spitzer archives[3]. First, we select science programs that probably includes PN observations from the list of science programs. Then we look into the Spitzer archives with the names of the science programs and obtain the list of Astronomical Observation Requests (AORs). We perform position search of the AORs one by one in SIMBAD, and obtain information about the target objects. We finally select 231 objects which are categorized in SIMBAD as "PN" and have information on the radial velocity. Since the number of objects is large, the list of selected PNe is given in a separate data file, "Spitzer-IRS_PN_Simbad_forSMI.csv". The list contains the name, position, Spitzer/IRS observation logs, and the properties of the objects. We also check the corresponding IRS spectra using the CASSIS archives[4], and obtain snapshots of the IRS spectra for 61 PNe out of 231 PNe available in the archive. We check the spectra and find that there are many PNe showing multiple and intense emission lines.

---

[2]https://www.nist.gov/
[3]https://irsa.ipac.caltech.edu/data/SPITZER/docs/spitzermission/observingprograms/
[4]https://cassis.sirtf.com

Table 2: List of emission lines covered with MR.

Order	$\lambda\,(\mu\mathrm{m})$	Planetary Nebula[1]	Be star[2]
m=11	18.0–18.9	[S III] 18.71 μm	HI 14 → 10 18.62 μm
m=10	18.9–20.8	[Fe II] 19.06 μm	HI 17 → 11 18.98 μm
		[Cl IV] 20.31 μm	HI 8 → 7 19.06 μm
			HI 20 → 12 20.51 μm
m=9	20.8–23.3	[Ar III] 21.83 μm	HI 16 → 11 20.92 μm
		[Fe III] 22.93 μm	HI 19 → 12 21.84 μm
		HI 13 → 10 22.33 μm	HI 13 → 10 22.33 μm
			HI 11 → 9 22.34 μm
m=8	23.3–26.3	[Ne V] 24.32 μm	HI 18 → 12 23.63 μm
		[Fe II] 24.52 μm	HI 15 → 11 23.87 μm
		[O IV] 25.89 μm	HI 17 → 12 26.17 μm
		[Fe II] 25.99 μm	
m=7	26.3–30.5	HI 9-8 27.80 μm	HI 20 → 13 26.68 μm
			HI 9 → 8 27.80 μm
			HI 14 → 11 28.83 μm
			HI 19 → 13 28.97 μm
		HI 12 → 10 29.85 μm	HI 12 → 10 29.85 μm
			HI 16 → 12 30.01 μm
m=6	30.5–36.0	[Fe III] 33.04 μm	HI 18 → 13 32.21 μm
		[S III] 33.48 μm	HI 20 → 14 35.04 μm
		[Si II] 34.82 μm	
		[Fe II] 35.35 μm	

(1) Lines presented here are those used for Spitzer IRS/LH calibration.
(2) H recombination lines taken from NIST Atomic Spectra Database Lines Data[6].

4.2.3   Be star candidates

Be stars show a variety of line profile depending on the disk geometry. It is also notable that Be stars may show time variation in line profile and its intensity. Since the spectral resolution of SMI/MR is as high as $R = 2600$ (i.e., $dv = 115\,\mathrm{km/s}$), MR can detect variations of line profile. Therefore, careful selection is necessary for Be stars considering the time variation of the line profile.

We search for objects which were observed with Spitzer/IRS from 2330 Be stars listed in the BeSS database[5] (Neiner et al. 2011). We use following two criteria for the selection. (i) More than 100 archival spectra are available (i.e. well studied object). (ii) Information on $v\sin i$ (i.e,, line width) is available. As a result, we find 187 Be stars observed with IRS, and 25 out of 187 stars were observed in LL and/or LH mode. We also include HD57150 ($v\sin i = 220\,\mathrm{km/s}$) in the candidate list as this star is a JWST/MIRI wavelength calibrator, although only six spectra are available. These selected 26 stars are listed in Table 3

Snapshot of the spectra for these 26 stars taken from CASSIS archive are presented in Appendix A.4 We find that 10 out of 26 stars show a series of hydrogen recombination lines. Figure 5 shows a Spitzer/IRS spectrum of HD57150 and its line identification. We confirm that all the recombination lines up to $n = 20$ in the NIST database[6] are detected. More lines can be identified by other line lists.

High stability of the line profile is required for the wavelength calibrators along the observation period. We also check the stability of the line profile for the candidate stars, because some Be stars are known to show significant time variations of the line profile. Hanuschik et al. (1996) reported the time variability of Hα obtained with high-velocity resolution spectroscopy in 1982–1993. Four out of 10 stars in our sample were studied in the paper. Figure 6 shows the time variation of the line profile for HD57150. We confirm that HD57150 shows a relatively stable emission line (i.e, variations of the line profile is small), although the spectrum shows a double-peaked profile. Figure 7 shows an example of Hα spectra of the other three Be stars. Especially 48 Lib shows significant time variation and is not preferable for a wavelength calibrator. Based on these results, we conclude that HD57150 is the best target for the wavelength calibration among the tested Be stars, and Alcyone is the second-best target.

---

[5] http://basebe.obspm.fr/basebe/
[6] https://physics.nist.gov/PhysRefData/ASD/lines_form.html

Table 3: List of Be stars selected as candidates of SMI wavelength calibration reference.

Name		Category	R.A.(J2000)	Dec.(J2000)	V[mag]	type	$v \sin i$	N_{spec}	Line
γ Cas		C	00 56 42.53	+60 43 00.27	2.47	B0IVpe	432	8995	H
ϵ Cas		C	01 54 23.73	+63 40 12.36	3.342	B3IIIe	30	526	
V777 Cas		C	01 55 42.85	+59 16 24.42	7.02	B2Vne	280	555	
HD 21362		C	03 28 52.33	+49 50 54.17	5.578	B6Vne	385	277	H
Electra	17 Tau	C	03 44 52.54	+24 06 48.01	3.705	B6IIIe	170	571	
Merope	23 Tau	C	03 46 19.57	+23 56 54.08	4.164	B6IVe	240	713	
Alcyone	η Tau	C	03 47 29.08	+24 06 18.49	2.873	B7IIIe	140	1090	H
Pleione	28 Tau	C	03 49 11.22	+24 08 12.16	5.048	B8IVev	290	8362	
Menkhib	ξ Per	C	03 58 57.90	+35 47 27.71	4.06	O7.5IIIe	213	4609	
43 Ori		C	05 35 22.90	−05 24 57.82	5.08	O9.5Vpe	183	291	
15 Mon		C	06 40 58.66	+09 53 44.72	4.64	B1Ve	70	1866	
V743 Mon		C	06 51 33.40	−06 57 59.45	6.583	B7IIIe	60	3348	
V742 Mon		C or H	06 51 45.75	+05 05 03.86	6.92	B2IIIe	181	148	H
HD 50658		C	06 56 32.06	+46 16 26.39	5.841	B8IIIe	235	222	
GU CMa		C or H	07 01 49.51	−11 18 03.32	6.58	B1.5Ve	352	333	H
HD57150	NV Pup	C	07 18 18.39	−36 44 02.23	4.7	B2Ve	220	6	H
β CMi		C	07 27 09.04	+08 17 21.54	2.886	B8Ve	230	851	H
θ CrB		C	15 32 55.78	+31 21 32.88	4.153	B6Vnne	340	3379	
V1040 Sco		C	15 53 55.86	−23 58 41.15	5.4	B2Ve	340	266	
4 Her		C	15 55 30.59	+42 33 58.29	5.74	B9pe	300	1835	H
48 Lib		C	15 58 11.37	−14 16 45.69	4.943	B8IIe	390	344	H
ζ Oph		C	16 37 09.54	−10 34 01.53	2.578	O9Ve	348	2660	
Sheliak	β Lyr	C	18 50 04.80	+33 21 45.61	3.52	B7Ve	120	2846	H
Alfirk	β Cep	C	21 28 39.60	+70 33 38.57	3.216	B2IIIev	20	8071	
ϵ Cap		C	21 37 04.83	−19 27 57.65	4.5	B3Vpe	225	215	
HD 206773		C	21 42 24.18	+57 44 09.80	6.927	B0Vpe	480	908	

Based on Neiner et al. (2011).

Categoly: C = Classical Be star, H = Herbig Be star

N_{spec}: Number of spectra collected in BeSS database.

Line: Targets showing strong Hydrogen recombination lines are indicated by 'H'.
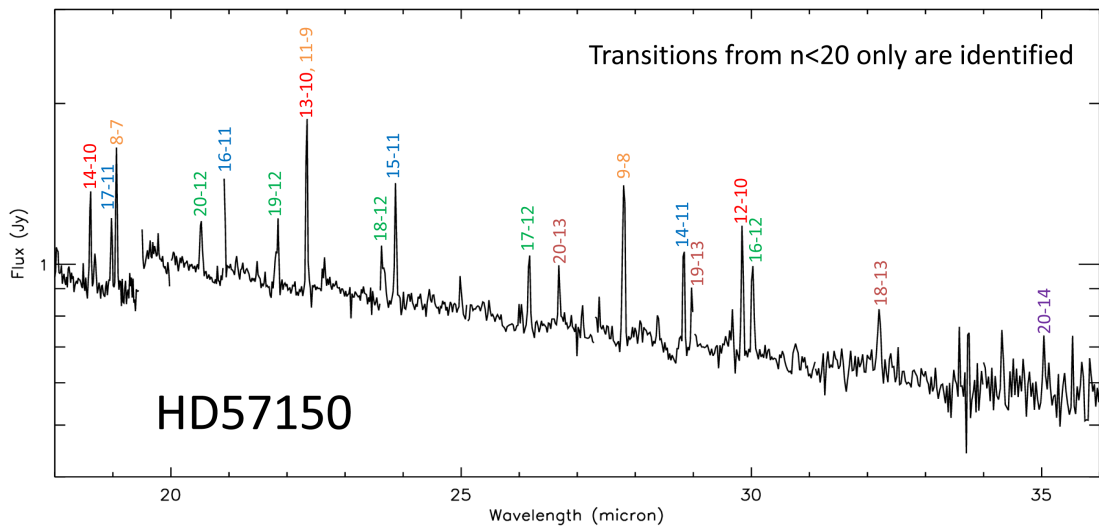
Figure 5: Spectrum of HD57150 with Spitzer/IRS.
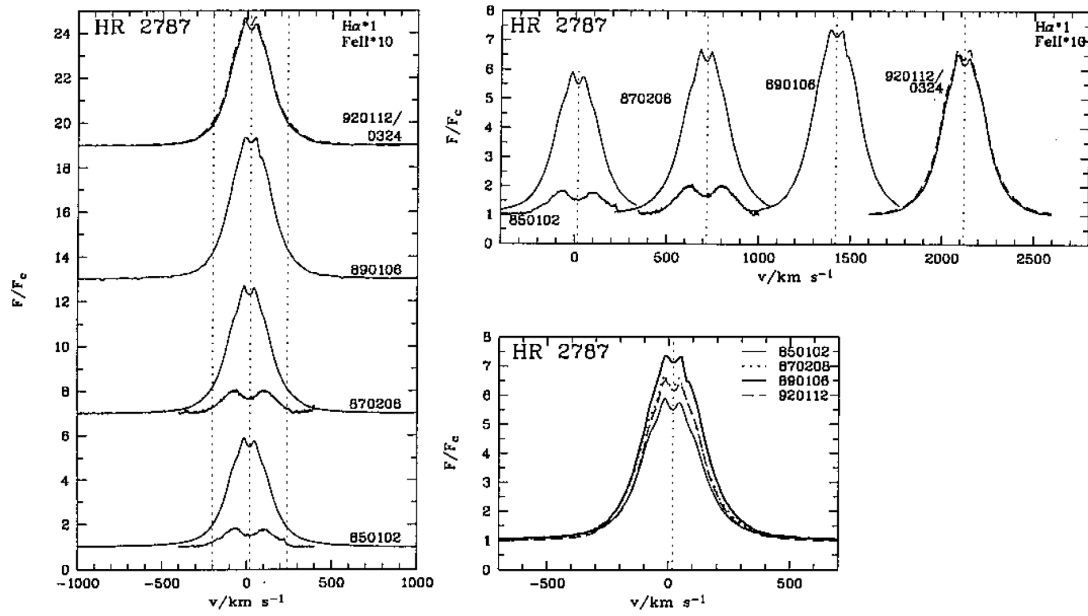
Figure 6: Time variation of the Hα line profile in HD57150 (HR2787) (Hanuschik et al. 1996). Reproduced with permission from Astronomy & Astrophysics, © ESO.
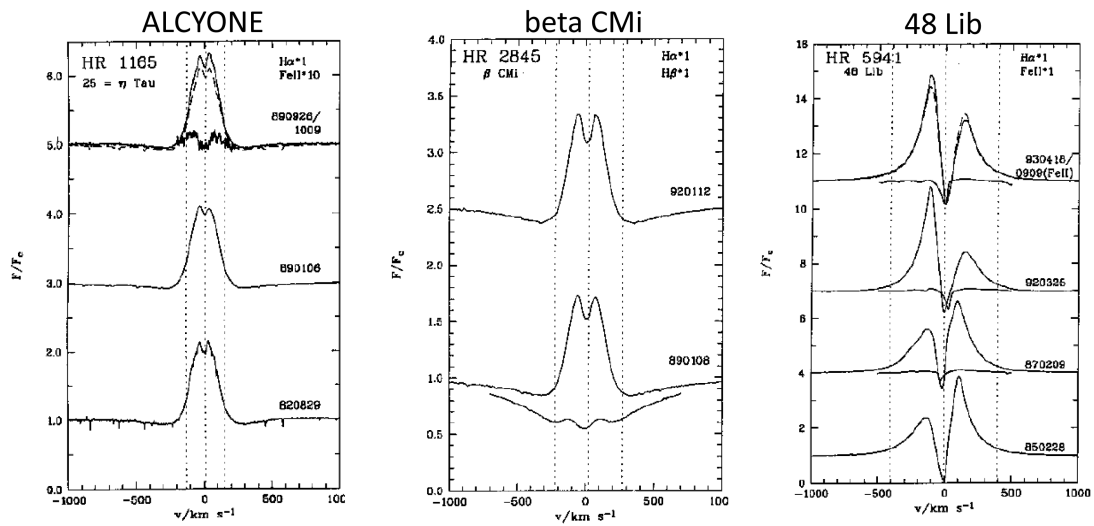
Figure 7: Line profile of Be stars (Hanuschik et al. 1996). Reproduced with permission from Astronomy & Astrophysics, © ESO.

4.3 Distortion correction

4.3.1 JWST calibration field for SMI

We check if the JWST reference field is applicable for the SMI distortion correction. First, we must recognize that the size of the JWST reference field is $5' \times 5'$, which is smaller than the FOV of SMI/CAM ($12' \times 10'$), because it is selected for the smaller FoV of JWST/MIRI ($74'' \times 113''$). The number count of stars located in the JWST reference field is summarized in Table 1 of Anderson (2008)[7]. To detect a sufficient number of stars (> 100 stars), stars as faint as magnitude $K \sim 14$ ($\sim 10\,\mu\mathrm{Jy}$ at $27\,\mu\mathrm{m}$) should be detected, which is too faint for the CAM sensitivity. Hence, the JWST calibration field is not preferable for the SMI distortion correction.

Figure 8 shows the surrounding environment of the JWST reference field. The JWST reference field is located at the center of LMC, where the number density of stars is large in near-infrared observations. The WISE W4 band ($22\,\mu\mathrm{m}$) map indicates that the JWST reference field is selected by avoiding nearby bright extended structures. These maps indicate that it is difficult to select a region that includes a larger number of bright stars than the JWST reference field. Hence, we conclude that LMC is not a suitable target for the SMI distortion correction.
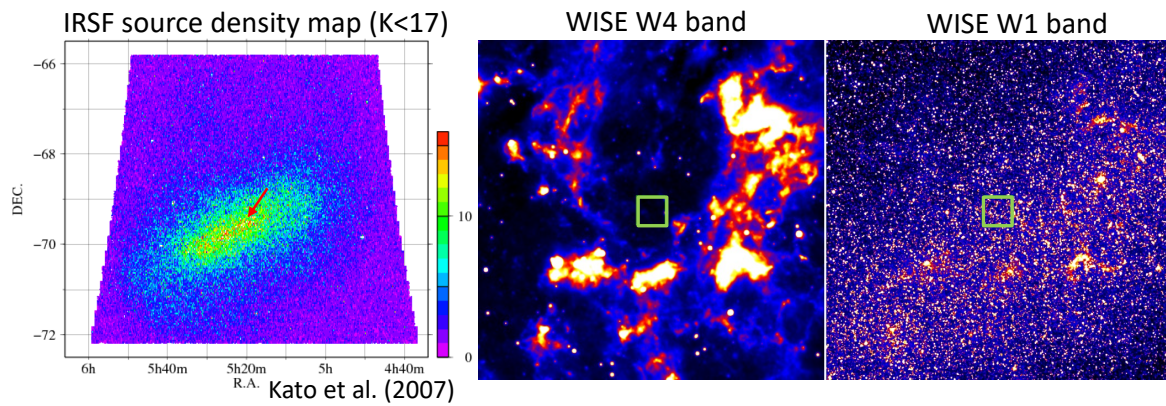
Figure 8: JWST reference field (red arrow or green box) in IRSF(Kato et al., 2007) and WISE data. The field of view of the WISE images is $1° \times 1°$.

4.3.2 Globular cluster

Candidates of globular clusters are selected from the list of 151 globular clusters[8] assembled from Harris (1996)[9] and Willman et al. (2005). Among these 151 objects, 29 objects have a diameter of $> 12'$ (i.e., SMI/CAM FOV size). Table 4 summarizes the properties of the 29 globular clusters. The number of point sources in the WISE and 2MASS point source catalogs, and the number density calculated from the number of point sources within the diameter of the cluster are also listed in the table.

We search for the globular clusters in the AKARI data archives and find that 10 out of 29 globular clusters were observed in L24 band. Figure 9 shows the AKARI L24 band images of these 10 globular clusters. We confirm that NGC 104 (47 Tuc) and NGC 5139 (ω Cen) extend beyond the SMI/CAM FOV, although the number density of the two objects is moderate as shown in Table 4.

We also check the WISE W1 and W4 band images of the 29 globular clusters shown in Figures 10 and 11. In W1 band, all the globular clusters look similar, while in W4 band images they are very different from object to object. Based on visual inspection of these images, we conclude that NGC 104 (47 Tuc), NGC 5139 (ω Cen), and NGC 6656 are the best targets for the distortion calibration. In terms of visibility, NGC 104 (47 Tuc) is the best, but still the object is only observable 40–70 days per year, depending on the configuration of the spacecraft.

---

[7] https://www.stsci.edu/files/live/sites/www/files/home/jwst/documentation/technical-documents/_documents/JWST-STScI-001378.pdf

[8] https://pages.uoregon.edu/imamura/123/exercises/Exercise_5_astr123.html

[9] https://physics.mcmaster.ca/~harris/Databases.html, 2003 Edition

Table 4: List of 29 globular clusters with a diameter of $> 12'$. The objects indicated by 'A' in "AKARI" column are observed by AKARI/IRC (See Figure 9).

Obj. name	RA (deg)	DEC (deg)	Diam. (arcmin)	Dist. (kLy)	N_{WISE}	N_{2MASS}	D_{WISE}	D_{2MASS}	AKARI
					(number of sources)		(sources/arcmin^2)		
NGC6205	250.425	36.467	20	25	5271	3489	4.2	2.8	A
NGC5024	198.225	18.167	13	58	2501	1157	4.7	2.2	A
NGC288	13.200	-26.583	13	29	2642	914	5.0	1.7	
NGC7089	323.375	-0.817	16	38	4007	2320	5.0	2.9	
NGC5904	229.650	2.083	23	24	8664	4285	5.2	2.6	
NGC5272	205.550	28.383	18	34	5408	2266	5.3	2.2	A
NGC7078	322.500	12.167	18	34	5470	3192	5.4	3.1	A
NGC6171	248.125	-13.050	13	21	3015	2416	5.7	4.6	
NGC6121	245.900	-26.533	36	7	23512	30363	5.8	7.5	
NGC6254	254.275	-4.100	20	14	7515	5365	6.0	4.3	
NGC6341	259.275	43.133	14	27	3734	1787	6.1	2.9	A
NGC4833	194.900	-70.867	14	21	3752	6246	6.1	10.1	
NGC6723	284.900	-36.633	13	28	3273	3865	6.2	7.3	
NGC3201	154.400	-46.417	20	16	7752	8992	6.2	7.2	A
NGC6752	287.725	-59.983	29	13	16424	11315	6.2	4.3	
NGC6218	251.800	-1.950	16	16	5080	3088	6.3	3.8	
NGC6809	295.000	-30.967	19	17	7259	7119	6.4	6.3	
NGC5139	201.700	-47.483	55	17	60898	57072	6.4	6.0	A
NGC104	6.025	-72.083	50	15	50703	24078	6.5	3.1	A
NGC6362	262.975	-67.050	15	25	4575	4636	6.5	6.6	
NGC6541	272.000	-43.500	15	23	4738	9399	6.7	13.3	
NGC362	15.800	-70.850	14	28	4132	2154	6.7	3.5	A
NGC2808	138.000	-64.867	14	31	4190	5114	6.8	8.3	A
NGC6656	279.100	-23.900	32	10	21938	65808	6.8	20.5	
NGC6266	255.300	-30.117	15	23	4936	15290	7.0	21.6	
NGC6397	265.175	-53.667	31	8	21086	31783	7.0	10.5	
NGC6273	255.650	-26.267	17	28	6344	15488	7.0	17.1	
NGC6366	261.925	-5.083	13	12	3785	4134	7.1	7.8	
NGC6626	276.125	-24.867	14	18	4710	13628	7.6	22.1	

Column "AKARI": 'A' means that AKARI data are available.
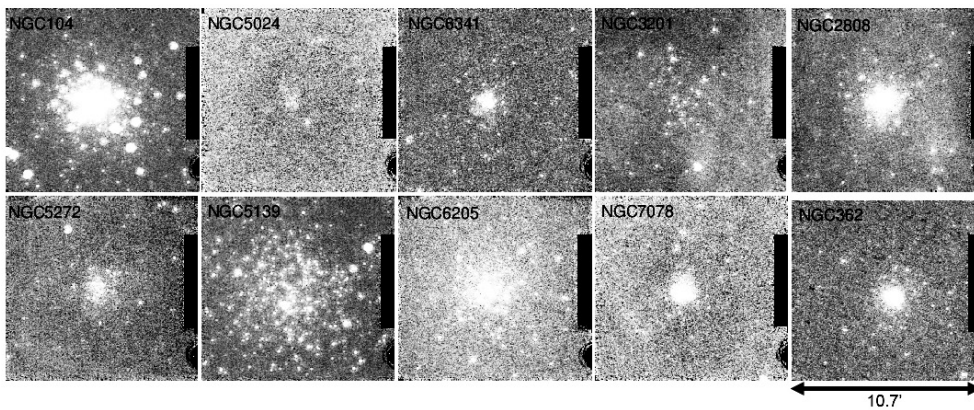
Figure 9: AKARI L24 images of 10 globular clusters indicated as 'A' in Table 4.

4.3.3 Open cluster

We also check the WISE W1 and W4 images of famous open clusters in the Messier catalog to judge if these open clusters are usable for the distortion correction of SMI/CAM. Figures 12 and 13 show the WISE images of 24 open
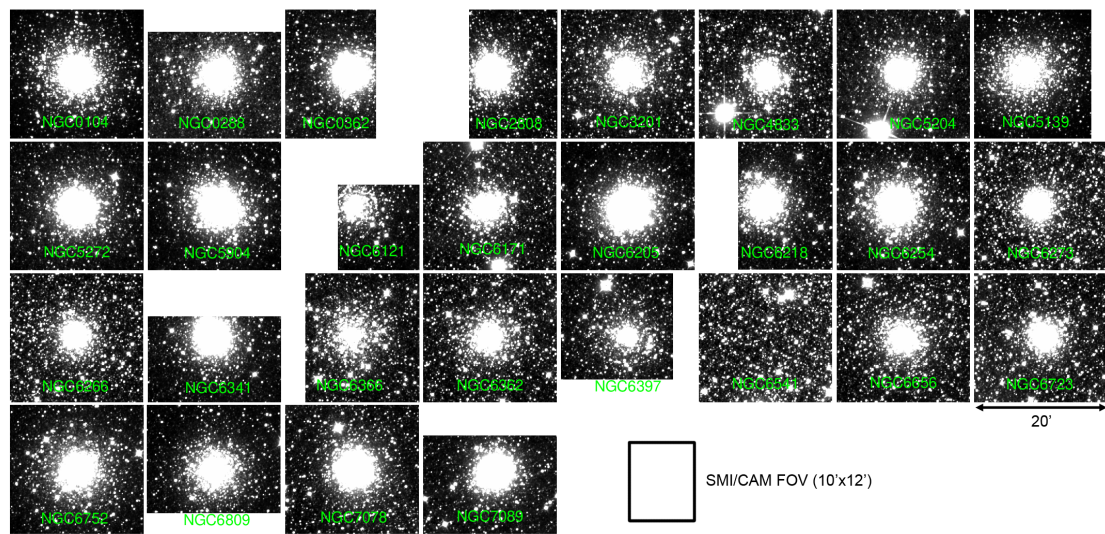
Figure 10: WISE W1 images of globular clusters. Size of each image is $20' \times 20'$.
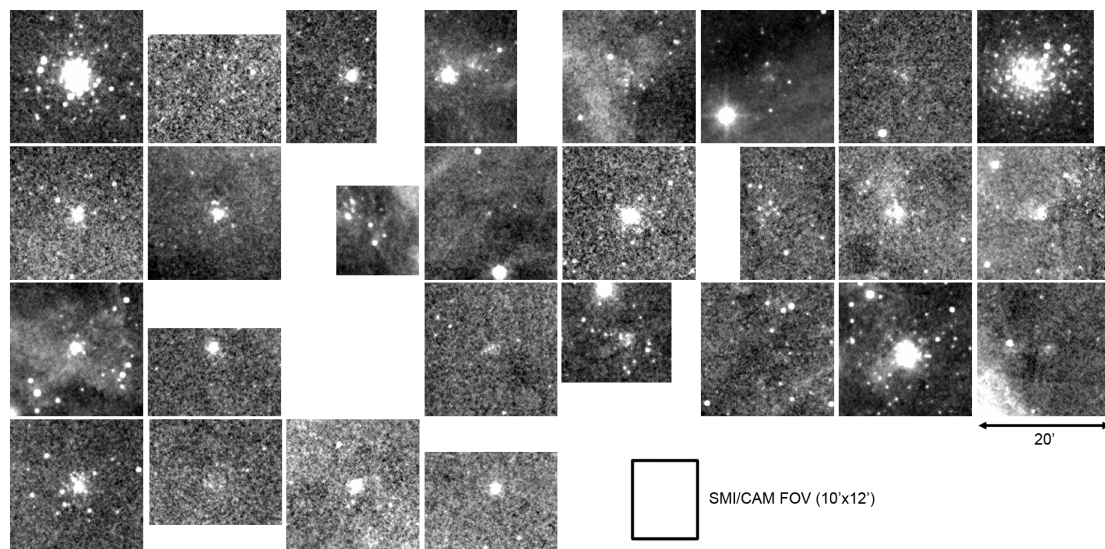
Figure 11: Same as Figure 10 but for WISE W4 band.

clusters in the Messier catalog. As in the case of globular clusters, a large number of stars are detected in W1 band, but the number of stars in W4 band is much smaller. In many cases, the number density of stars in open clusters in a mid-infrared wavelength range is insufficient for our purpose. In addition, open clusters are typically located on the Galactic plane, which indicates that the observation visibility is low. Hence we conclude that open clusters are not good for the distortion correction.
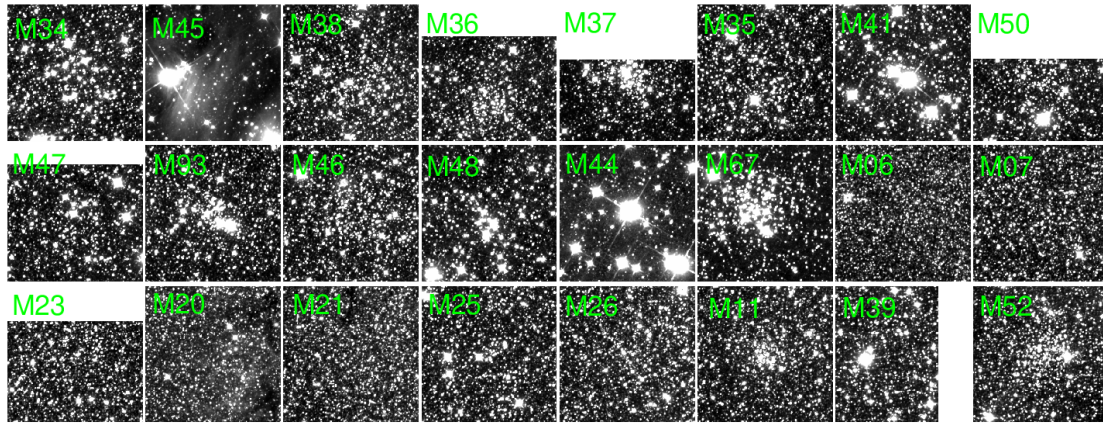
Figure 12: WISE W1 band images of open clusters in Messier catalog. Size of each image is $20' \times 20'$.
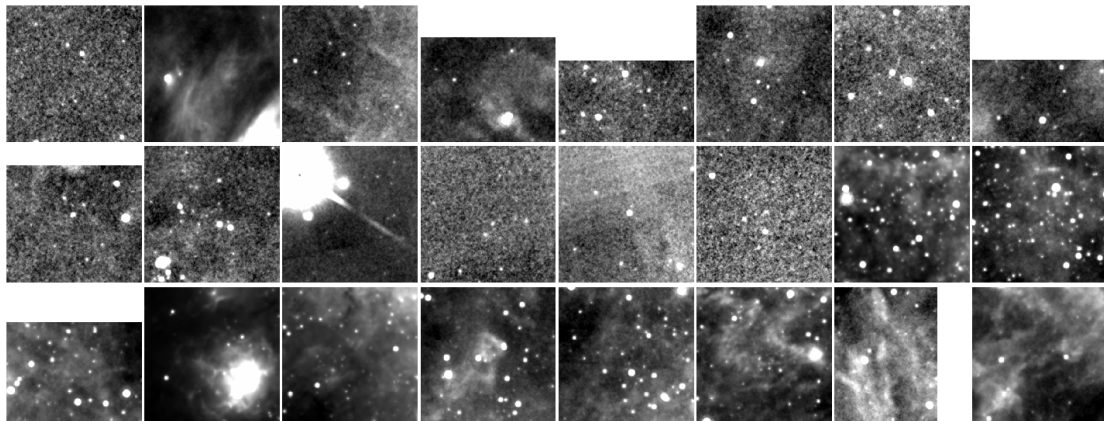
Figure 13: Same as Figure 12 but for WISE W4 band.

5   Summary

We have considered calibration strategies and suitable celestial objects for the in-flight calibration of SPICA/SMI. Our main results are summarized as follows.

- For the flux calibration, the calibration standard stars established for Spitzer/IRS and JWST/MIRI can be applied for SMI. The use of these established stars is also useful for cross-calibration between the instruments. In addition, Uranus or Neptune shall be observed to check leakage of short-wavelength light in the data.

- The wavelength calibration for SMI/MR and LR can be done by observing PNe and Be stars. Both types of objects have advantages and disadvantages and a combination of the two types of objects is recommended. There are sufficient number of sources available in the sky.

- We show that ro-vibrational lines of H_2O, CO_2, HCN, and C_2H_2 can be used for the wavelength calibration of SMI/HR channel, in which a spectrum is split into many segments. However, more detailed studies as well as ground-based observations are needed to establish this calibration scheme.

- The correction of geometric distortion of the focal-plane image is attempted by three different methods. It is found that the free-form mirror based focal-plane of SMI is rather difficult to model with a small number of reference points. Empirical modeling by cubic-interpolation with far more than one hundred reference points may achieve the required accuracy, but it should be confirmed by future studies. Globular clusters are the most suitable objects for the reference, but the number of objects that can provide a sufficient number of stars in the mid-infrared is limited.

- We estimate the amount of observing time for the calibration, and find that it fits the allocated calibration time, i.e., 10% of the total observing time.

Unfortunately, SPICA mission we have considered will not be realized and the calibration plan we discuss here will not be applied as it is. We expect that our results will be useful for calibration of future infrared astronomical missions.

Acknowledgements

References

Anderson, J. 2008, JWST Technical Report, JWST-STScI-001378, SM-12. `https://www.stsci.edu/files/live/sites/www/files/home/jwst/documentation/technical-documents/_documents/JWST-STScI-001378.pdf`

Arimatsu, K., Onaka, T., Sakon, I., et al. 2011, PASP, 123, 981

Bohlin, R. C., & Cohen, M. 2008, AJ, 136, 1171

Cohen, M., Megeath, S. T., Hammersley, P. L., Martín-Luis, F., & Stauffer, J. 2003, AJ, 125, 2645

Cohen, M., Walker, R. G., Carter, B., et al. 1999, AJ, 117, 1864

Decin, L., Morris, P. W., Appleton, P. N., et al. 2004, ApJS, 154, 408

Engelbracht, C. W., Blaylock, M., Su, K. Y. L., et al. 2007, PASP, 119, 994

Hanuschik, R. W., Hummel, W., Sutorius, E., Dietle, O., & Thimm, G. 1996, A&AS, 116, 309

Harris, W. E. 1996, AJ, 112, 1487

Holtzman, J. A., Hester, J. J., Casertano, S., et al. 1995, PASP, 107, 156

Houck, J. R., Roellig, T. L., van Cleve, J., et al. 2004, ApJS, 154, 18

IRS Instrument Team & Science User Support Team. 2011, Spitzer Heritage Archive Documentation. https://irsa.ipac.caltech.edu/data/SPITZER/docs/irs/irsinstrumenthandbook/

Kato, D., Nagashima, C., Nagayama, T., et al. 2007, PASJ, 59, 615

Kessler, M. F., Steinz, J. A., Anderegg, M. E., et al. 1996, A&A, 315, L27

Kondo, T., Ishihara, D., Kaneda, H., et al. 2016, AJ, 151, 71

Murakami, H., Baba, H., Barthel, P., et al. 2007, PASJ, 59, S369

Neiner, C., de Batz, B., Cochard, F., et al. 2011, AJ, 142, 149

Neugebauer, G., Habing, H. J., van Duinen, R., et al. 1984, ApJL, 278, L1

Ohyama, Y., Onaka, T., Matsuhara, H., et al. 2007, PASJ, 59, S411

Partridge, H., & Schwenke, D. W. 1997, The Journal of Chemical Physics, 106, 4618

Pilbratt, G. L., Riedinger, J. R., Passvogel, T., et al. 2010, A&A, 518, L1

Pottasch, S. R., Bernard-Salas, J., & Roellig, T. L. 2007, A&A, 471, 865

Rinsland, C. P., Baldacci, A., & Rao, K. N. 1982, ApJS, 49, 487

Roelfsema, P. R., Shibai, H., Armus, L., et al. 2018, PASA, 35, e030

Rothman, L. S., Gordon, I. E., Barbe, A., et al. 2009, Journal of Quantitative Spectroscopy and Radiative Transfer, 110, 533

Sloan, G. C., Herter, T. L., Charmandaris, V., et al. 2015, AJ, 149, 11

Tanabé, T., Sakon, I., Cohen, M., et al. 2008, PASJ, 60, S375

Tauber, J., & SPICA Science Study Team. 2021, SPICA-EST-SCI-RS-001

Wada, T., Kaneda, H., Kokusho, T., et al. 2020, in SPIE Conference Series, Vol. 11443, 114436G

Werner, M. W., Roellig, T. L., Low, F. J., et al. 2004, ApJS, 154, 1

Willman, B., Blanton, M. R., West, A. A., et al. 2005, AJ, 129, 2692

Wright, E. L., Eisenhardt, P. R. M., Mainzer, A. K., et al. 2010, AJ, 140, 1868

Yamamura, I., de Jong, T., & Cami, J. 1999, A&A, 348, L55

Yamamura, I., de Jong, T., Justtanont, K., Cami, J., & Waters, L. B. F. M. 1998, Ap&SS, 255, 351

A Appendix

A.1 Calibration targets for AKARI, Spitzer, and JWST

A.1.1 Absolute flux

Information on absolute flux calibration in AKARI, Spitzer, and JWST is summarized below.

- Spitzer/MIPS $24\,\mu$m
  - Standard stars: 141 objects ($8.6\,$mJy–$4.0\,$Jy @$24\,\mu$m)
  - Exposure time: 3 sec
  - Calibration process is summarized in Engelbracht et al. (2007)

- Spitzer/IRS
  - low-res primary standard: HR 7341 $\cdots$ $0.2\,$Jy @$27\,\mu$m, $0.6\,$Jy @$15\,\mu$m
  - high-res primary standard: HR 6688 $\cdots$ $2.3\,$Jy @$27\,\mu$m, $7.5\,$Jy @$15\,\mu$m
  - other standard stars: K giant 33 objects (0.37–$1.25\,$Jy @$12\,\mu$m), A dwarf 20 objects (0.08–$0.96\,$Jy @$12\,\mu$m), M giant 20 objects (0.87–$2.95\,$Jy @$12\,\mu$m)
  - Calibration process is summarized in Sloan et al. (2015)
  - Stellar model of standard stars: Decin et al. (2004)

- AKARI/IRC imaging
  - NEP standard (A, K type stars)
    * K = 5.7–11.1 mag (for NIR/MIR-S) $\rightarrow$ 0.2–$30\,$mJy @$27\,\mu$m
    * K = 4.0–8.1 mag (for MIR-L) $\rightarrow$ 3–$140\,$mJy @$27\,\mu$m
  - SAGE standard (A, K, M type stars)
    * K = 4.0–10.7 mag (for NIR/MIR-S) $\rightarrow$ 0.3–$140\,$mJy @$27\,\mu$m
    * K = 4.0–8.6 mag (for MIR-L) $\rightarrow$ 2–$140\,$mJy @$27\,\mu$m
  - Stellar model: Cohen et al. (2003)
  - Reference: Tanabé et al. (2008)

- AKARI/IRC spectroscopy
  - A, K type stars: K = 3.6–11.7 mag $\rightarrow$ 0.1–$200\,$mJy @$27\,\mu$m
  - Stellar model: Cohen et al. (2003)

- JWST/MIRI imaging+spectroscopy
  - See Table 5
  - BD+60-1753 and HD163466 will be observed 11 times during Cycle 1 to check repeatability.
  - Absolute flux calibration will be performed in program ID: 1536–1539.

Table 5: List of flux calibrators for JWST/MIRI

Obj. name	Spec. type	K (mag)	Image	LRS	MRS
1743045	A5V	12.772	✓		
1802271	A3V	11.832	✓		
1812095	A2V	11.286	✓		
BD+60-1753	A1V	9.64	✓(*)	✓	
HD180609	A3V	9.12	✓	✓	
HD002811	A3V	7.04	✓	✓	✓
HD163466	A6V	6.34	✓		✓(*)
del-Umi	A1V	4.26	✓		✓
P177D	G2V	11.857	✓		
P330E	G2V	11.379	✓	✓	
HD167060	G2V	7.43	✓	✓	✓
HD38949	G1V	6.44	✓	✓	
HD37962	G2V	6.27	✓	✓	✓
16 Cyg B	G2/3V	4.66	✓		✓
G191B2B	DA0	12.764	✓		
GD153	DA1	14.308	✓		
GD71	DA1	14.115	✓		

(*) BD+60-1753 and HD163466 will be observed 11 times in imaging and MRS, respectively, for the confirmation of the repeatability.

A.1.2 Wavelength

Information on wavelength calibration in AKARI, Spitzer, and JWST is summarized in Table 6.

Table 6: Targets used for wavelength calibration

Instrument	Object type	Object name	Flux	Note
Spitzer/IRS	PN	M1-42	1.0 Jy @27 μm	Extended
Spitzer/IRS	PN	NGC7293	0.08 Jy @27 μm	Central star of PN
Spitzer/IRS	PN	NGC6543	30 Jy @27 μm	Extended
AKARI/IRC MIR-S	PN	NGC6543		Extended
AKARI/IRC MIR-S	WR star	WR128	K=9.6	
AKARI/IRC MIR-S	WR star	NGC6543	K=6.2	
AKARI/IRC MIR-L	galaxy	Mrk 3		
JWST/MIRI MRS	Be star	HD57150	K=4.6	Main calibrator
JWST/MIRI LRS	Be star	HD50083	K=6.5	Sub calibrator
JWST/MIRI LRS	LP variable	J05213020-6931544	K=11.5	Sub calibrator
JWST/NIRSpec	PN	NGC6543		
JWST/NIRCAM	PN	unresolved PN @LMC	K=14.5	

A.1.3 Distortion

Information on distortion correction in AKARI, Spitzer, and JWST is summarized in Table 7.

Table 7: Targets used for distortion correction

Instrument	Object type	Object name
Spitzer/IRAC	Globular cluster	NGC 6791, NGC 2420
AKARI/IRC	Globular cluster	47 Tuc (NGC 104)
JWST/MIRI		Reference field @LMC (5'x5') (*)

(*) Positional information on 200,000 stars is available for the JWST calibration field with positional accuracy of 1 mas based on HST/ACS observations.

A.2   Calibration time in previous space IR missions

Calibration time and achieved flux/wavelength accuracy in AKARI, Spitzer, and Herschel are summarized in Tables 8, 9, 10. Information of calibration observations are collected mainly from their observation log. [10] [11] [12] In the previous missions, a typical fraction of calibration time is ~10 % of the total observation time.

Table 8: Summary of calibration time in AKARI.

Channel	$N_{obs.}$	$N_{std.}$		$N_{mon.}$	$F_{cal.}$	Accuracy
		NEP/SEP	SAGE			
NIR/MIR-S	2324	16 (14)	27 (24)	34 (1)	3.3 %	2.5–6.0 %
MIR-L	824	9 (9)	25 (21)	31 (2)	7.9 %	
Total	3148	25 (21)	52 (26)	65 (2)	4.5 %	

Imaging[a]

Channel	$N_{obs.}$	$N_{std.}$		$N_{mon.}$	$F_{cal.}$	Accuracy
		Flux	Wavelength			
NIR/MIR-S	700	19 (7)	6 (3)	16 (1)	5.9 %	Flux: 10%
MIR-L	239	3 (3)	1 (1)	17 (2)	8.8 %	Wavelength: 0.2% (NG)
Total	939	22 (7)	7 (3)	33 (2)	6.6 %	0.5% (Others)

Spectroscopy[b]

[a] Data from Tanabé et al. (2008).
[b] Data from Ohyama et al. (2007).
$N_{obs.}$: Total number of observations executed in Phase 1& 2 (cryogenic phase). Considered AOTs are IRC00, IRC02, IRC03, and IRC05 for imaging and IRC04 for spectroscopy. The exposure time of an observation is 10–20 minutes.
$N_{std.}$: Number of observations of standard stars and the number of objects in parentheses.
$N_{mon.}$: Number of monitoring observations and the number of monitoring fields in parentheses.
$F_{cal.}$: Fraction of calibration observations (($N_{std.} + N_{mon.}$)/$N_{obs.}$).

[10] https://irsa.ipac.caltech.edu/data/SPITZER/docs/spitzermission/observingprograms/observinglogs/
[11] http://herschel.esac.esa.int/obslog/Obslog.html
[12] http://herschel.esac.esa.int/obslog/Obslog.html?cal
[13] https://irsa.ipac.caltech.edu/data/SPITZER/docs/mips/mipsinstrumenthandbook/

Table 9: Summary of calibration time in Spitzer Space Telescope (observation time in unit of hours).

Instrument	(1)	(2)	(3)	(4)	(5)	(6)	(7)
IRAC	11,587	232	164	—	397 (3.4%)	Flux:3%[a] Repeatability: 1%	1,570 (13.5 %)
IRS spec	16,444	140	662	88	890 (5.4%)	Flux:20% Wavelength:FWHM/5 Low-res. 0.1% High-res. 0.01%	2,224 (13.0%)
IRS PUI	599	92	40	—	132 (22.1%)	Flux: 2% Repetability: 1-2%	
MIPS photo	11,953	100	264	—	364 (3.0%)	Flux:5, 10, 12 % Repeat.:1, 7, 10 % for 24, 70, 160 μm	991 (8.0%)
MIPS SED	460	5.4	70	?[b]	75 (16.4%)	Flux: 10%(point), 15% (extended) Repeatability < 5% Wavelength:∼2%	

(1) Total observation time without the instrument engineering observations, (2) The observation time for flux calibration and monitors with the primary calibrators, (3) The observation time of the flux confirmations, (4) The observation time of the wavelength calibrations, (5) Total time of the calibrations without dark and flat measurements, (6) Achieved accuracy from the instrument handbook of each instrument, and (7) Total time for the calibrations with dark and flat measurements

[a] The accuracy is limited by the stellar spectral models.

[b] MIPS Instrument Handbook[13] notes five objects were used for calibration, but we could not identify corresponding observations in the log data.

Table 10: Summary of calibration time in Herschel Space Observatory. (observation time in unit of hours)

Instrument	(1)	(2)	(3)	(4)	(5)	(6)	(7)
PACS photo	6,532	37	441	—	478 (7.3 %)	Flux:5%[a] Repeatability: 2%	764 (11.7%)
PACS spec	6,615	423	572	79	1073 (16.2%)	Flux:12% Repeatability:4% Wavelength:FWHM/10	1,138 (17.2%)
SPIRE photo	5,659	91	582	—	673 (11.9 %)	Flux:4%[a] Repeatability: 1.5%	971 (17.2%)
SPIRE spec	2,559	44	296	44	384 (15.0 %)	Flux:3%[a] Repeatability: 1% Wavelength:FWHM/10	842 (32.9%)
HIFI		chopper wheel				Flux:1.6-6% Repeatability:2-12% Wavelength:FWHM/10	

(1) Total observation time for science and calibration (without engineering observation), (2) Observation time for the flux calibration and monitoring observation with the primary calibrators, (3) The observation time of the flux confirmation, (4) The observations time of the wavelength calibration, (5) The total observation time for the calibrations without engineering observations, (6) Achieved accuracy from Herschel overview explanatory supplement, and (7) The total observation time for the calibrations including engineering observations.

[a] The accuracy is limited by the stellar spectral models.

A.3   Molecular lines for HR wavelength calibration

In this section we describe the result of a simple simulation to assess the possibility of using molecular lines for HR wavelength calculation by observing red-giant stars.

There are many bright red-giant stars in the sky. They are often pulsating variables such as Mira type or Semi-regular types. Their effective temperature is as low as 3000 K or even less, allowing to form various molecules in the atmosphere. Ro-vibrational transition lines of these molecules are observed in the near- to mid-infrared wavelength range in absorption or sometimes in emission. In the wavelength range of SMI/HR, 10–$18\,\mu$m, major molecules that are expected to show spectral bands are H_2O and CO_2 in oxygen-rich environment, and HCN and C_2H_2 in carbon-rich environment (i.e., carbon stars).

A set of simple numerical simulations are carried out. For simplicity we use plane-parallel configuration. The continuum radiation from the star is expressed by the black-body of 3000 K. A molecular layer with given column density N and excitation temperature T_{ex} is located on top of the continuum source, and the absorption spectra are calculated. The parameters and used line list are summarized in Table 11. These values are given as 'reasonable assumption' from the experiences in previous studies (e.g., Yamamura et al., 1999, 1998). The calculated spectra are smoothed with a Gaussian kernel corresponding to $R = 30,000$.

Table 11: Parameters for molecular absorption lines.

Molecule	N (cm^{-2})	T_{ex} (K)	Data Source
H_2O	1×10^{-20}	1,000	Partridge & Schwenke (1997)
CO_2	1×10^{-18}	1,000	Rothman et al. (2009) (HITENP2010)
HCN	1×10^{-18}	1,000	Rothman et al. (2009) (HITRAN2008)
C_2H_2	1×10^{-18}	1,000	Rinsland et al. (1982)

Figure 14 shows the results. Each pair of blue or red lines and numbers on the top of the plot indicates the wavelength range of an Echelle order. The spectrum is normalized by the continuum level. H_2O lines presents over the entire HR wavelength range, which may be used as wavelength reference. In addition, other molecules show lines in mainly 13–$17\,\mu$m that can be used to cross-check the results. We must admit that the current simulation is simple and preliminary. Further assessment by more realistic models as well as possible ground-base observations are needed to establish this calibration scheme.
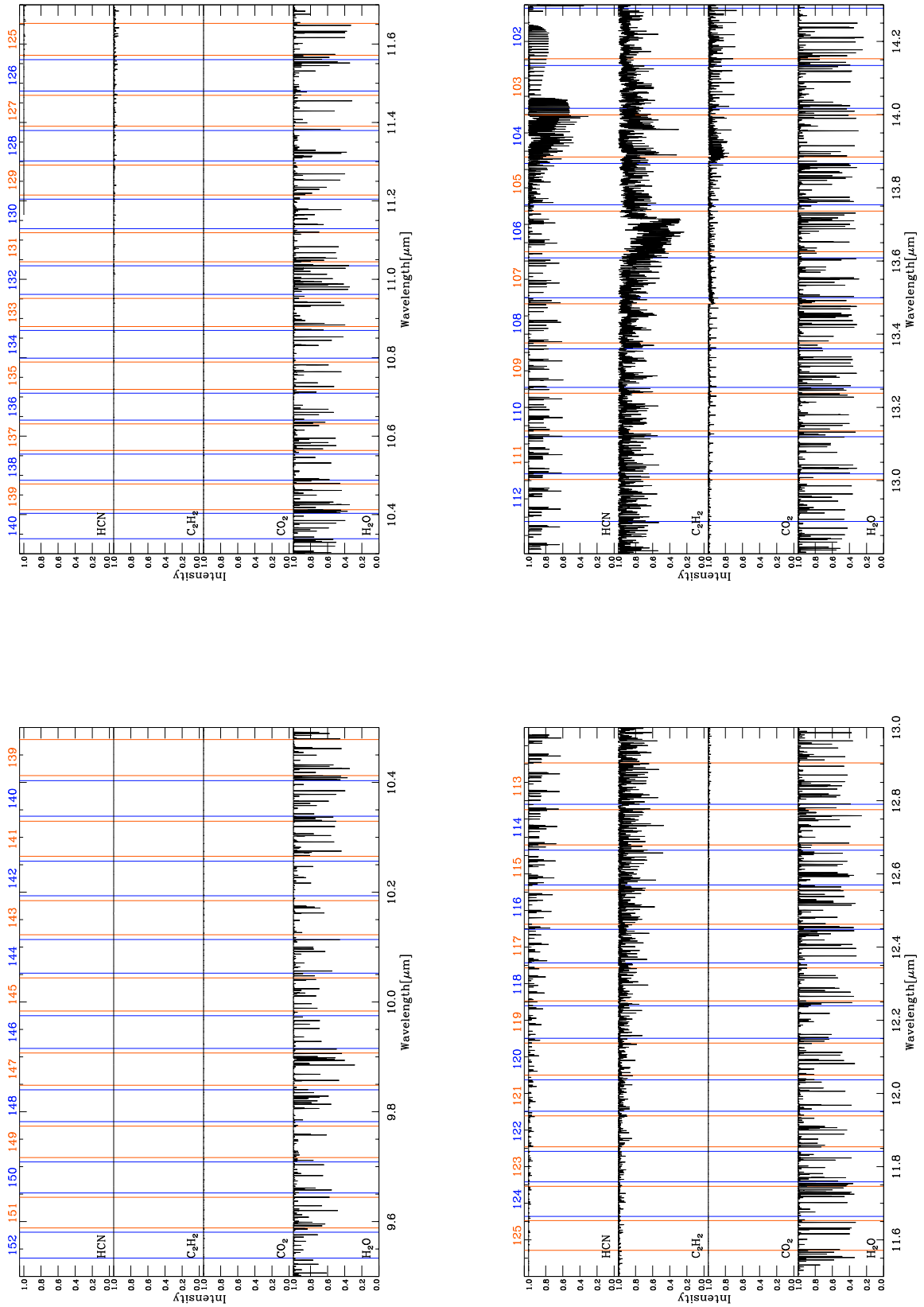
Figure 14: Results of molecular absorption lines in the wavelength range of SMI/HR. Plane-parallel configuration is adopted. Each pair of blue or red lines and numbers on top of the figure represents the range of an Echelle order.
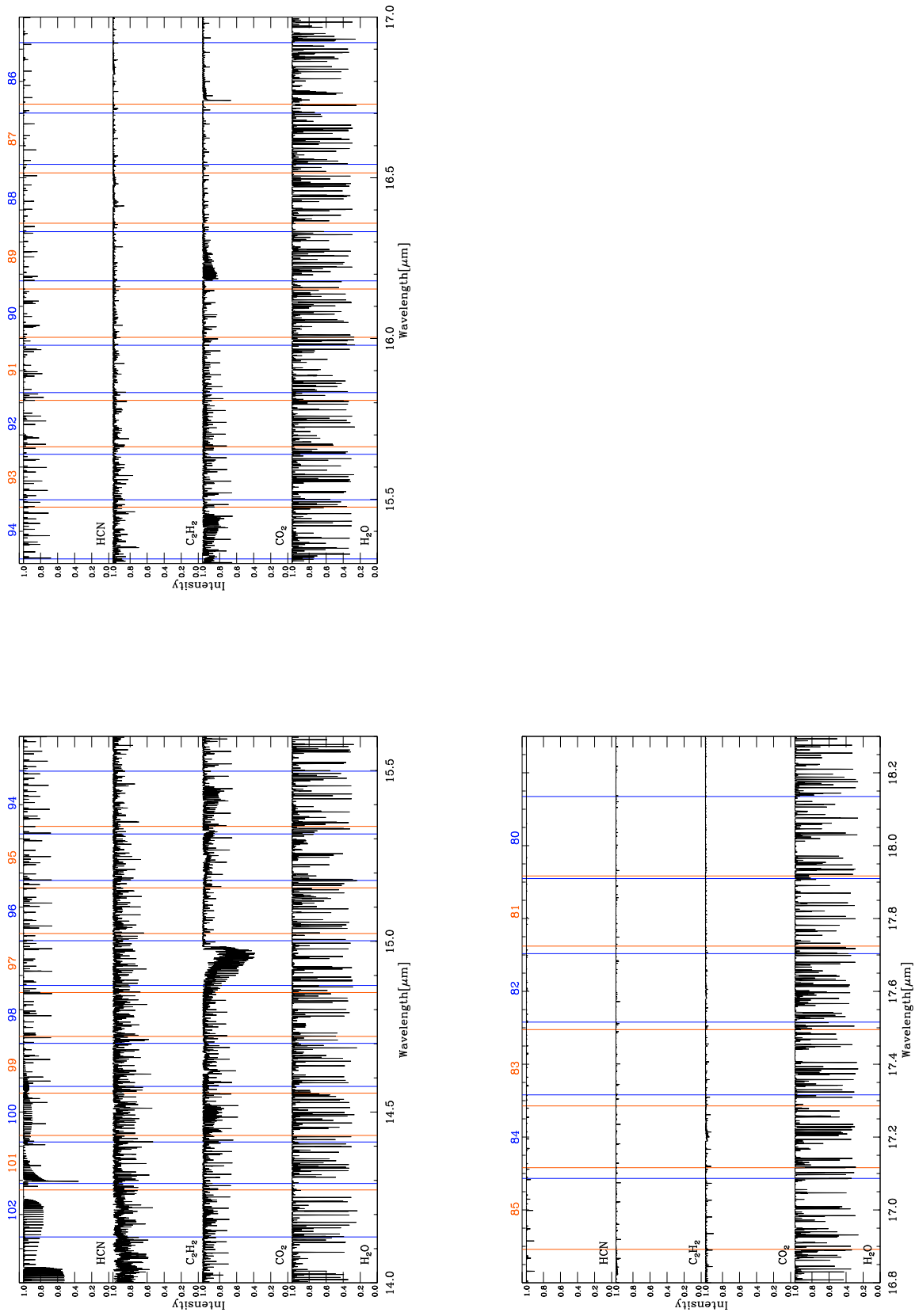
Figure 14: *Continued.*

A.4 Infrared spectra of Be Stars

Infrared spectra of Be stars possibly used for the wavelength calibration of SMI are presented in Figure 15. Plots are Quick-Look images from CASSIS database and IRSA. We can identify sources with strong emission lines.
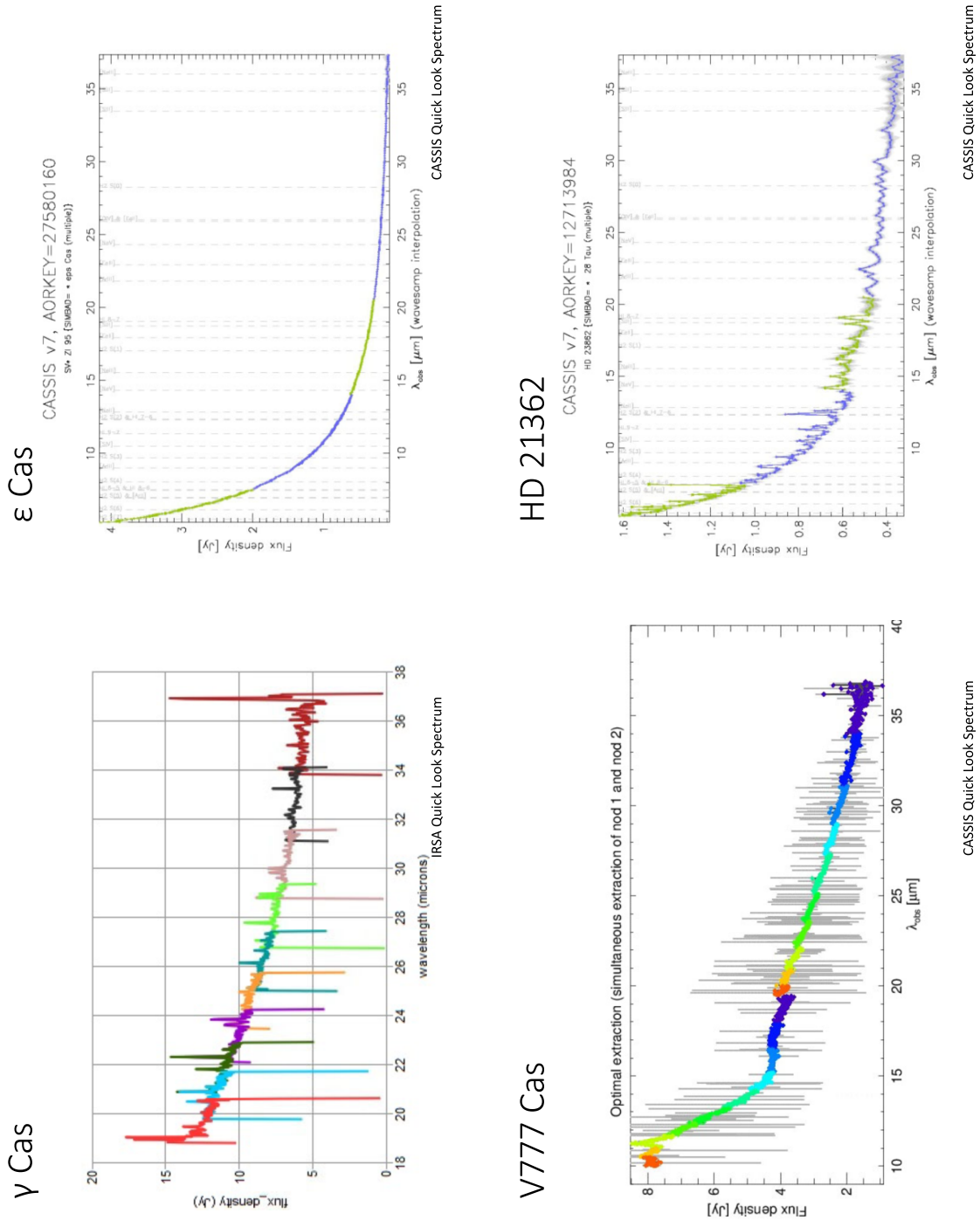
Figure 15: Snapshot spectra of Be Stars taken from CASSIS or IRSA.
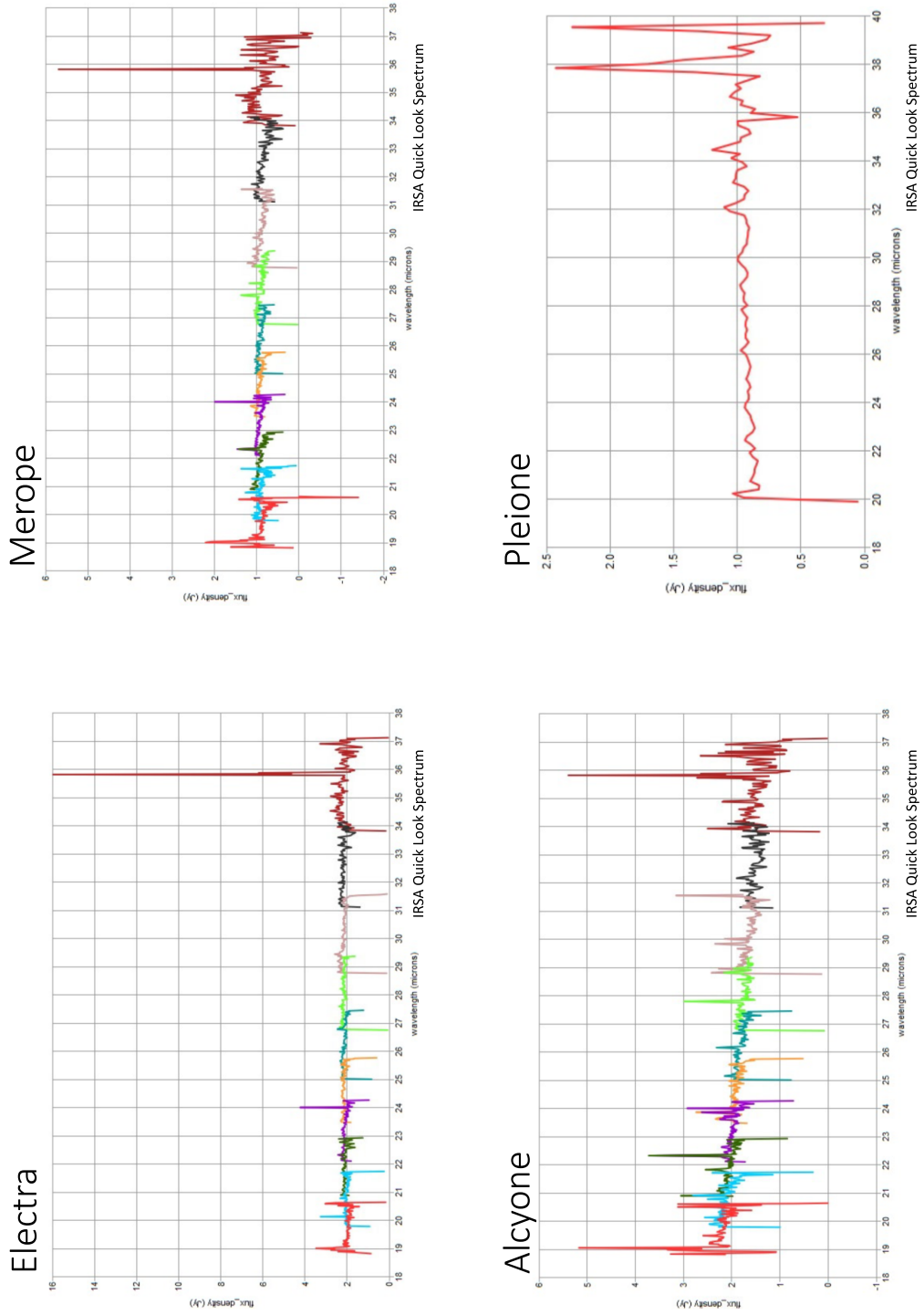
Figure 15: *Continued*
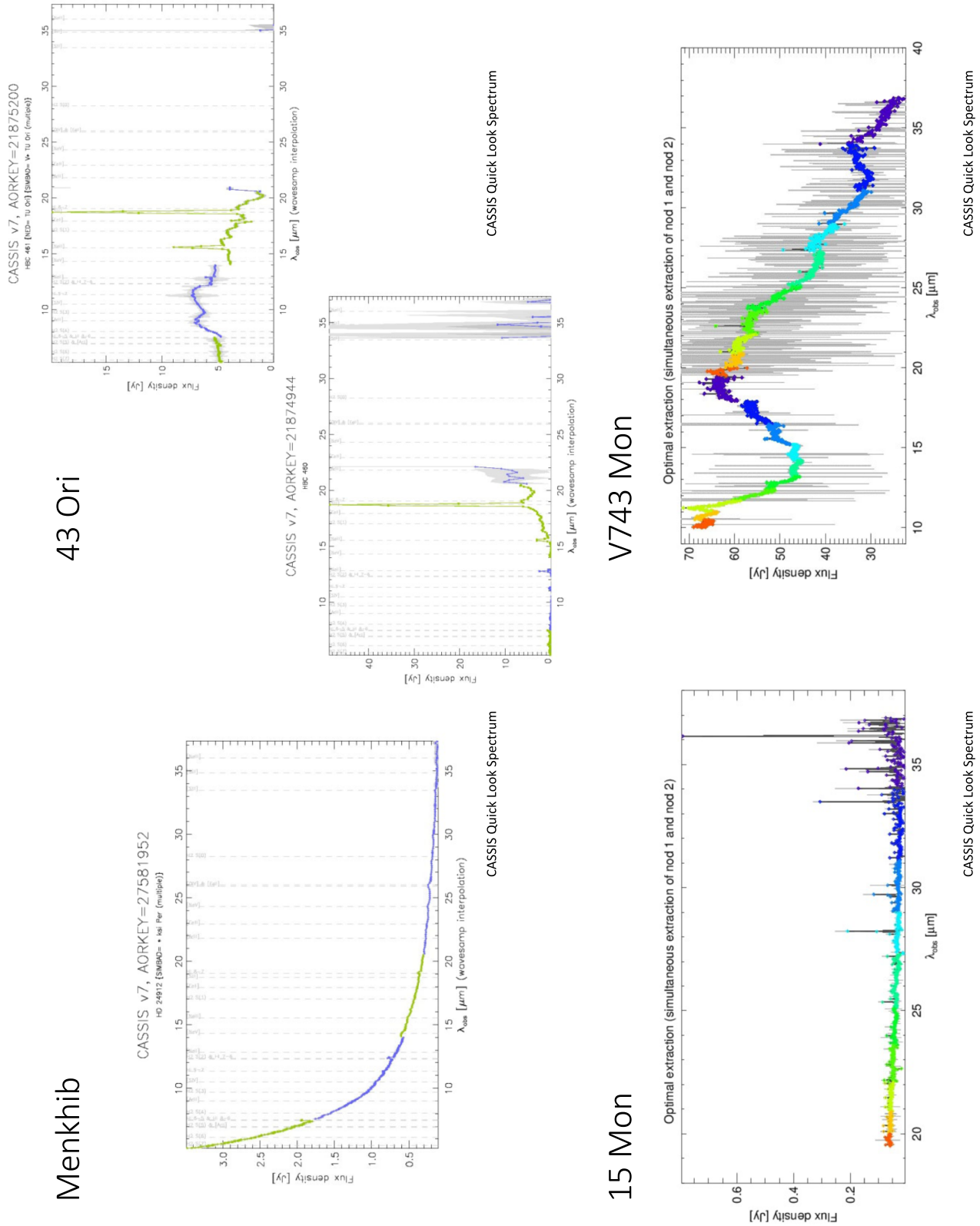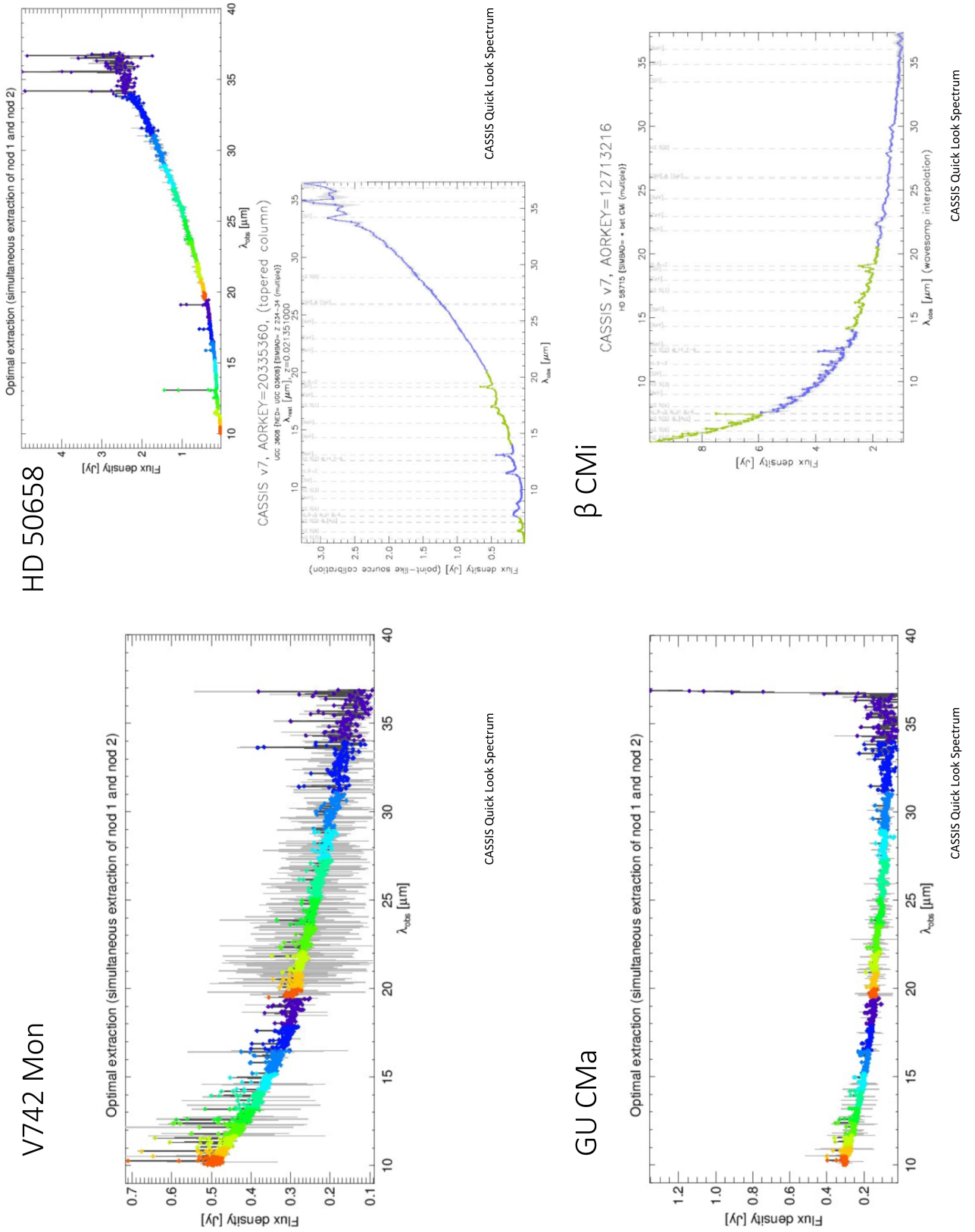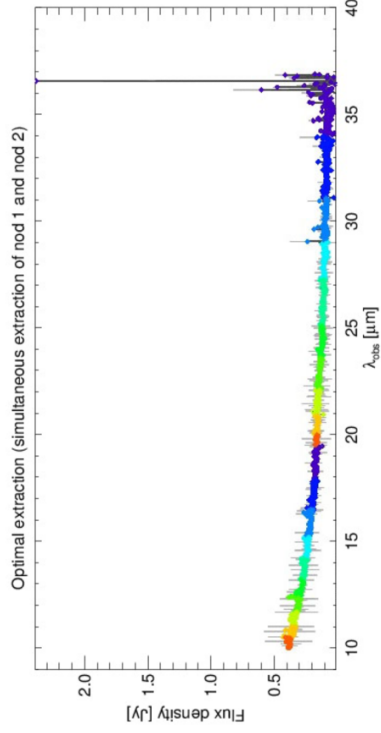
Figure 15: *Continued*

Figure 15: *Continued*

Figure 15: *Continued*

Sheliak

ζ Oph

ε Cap

Alfirk
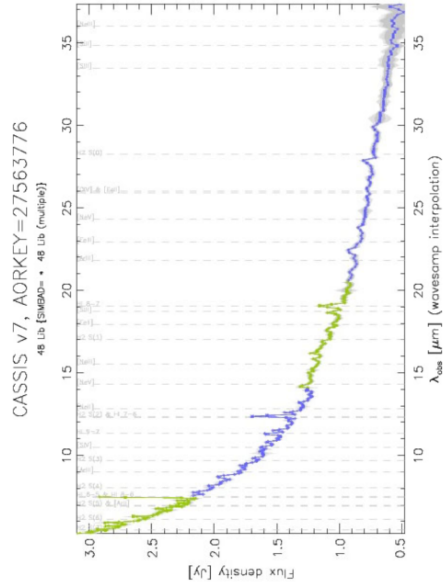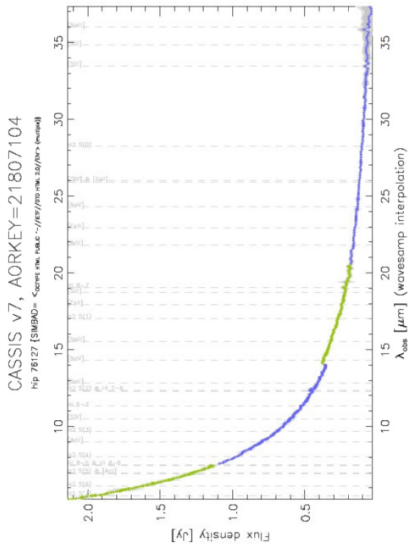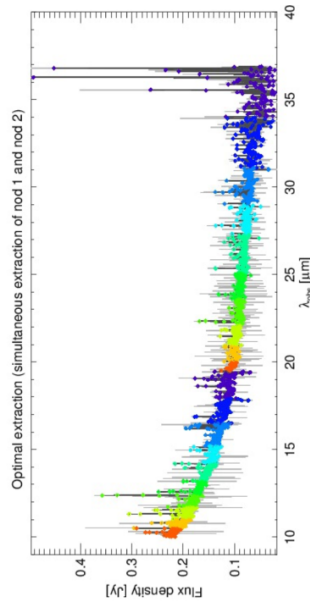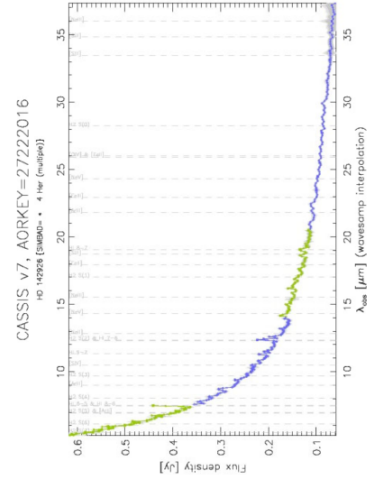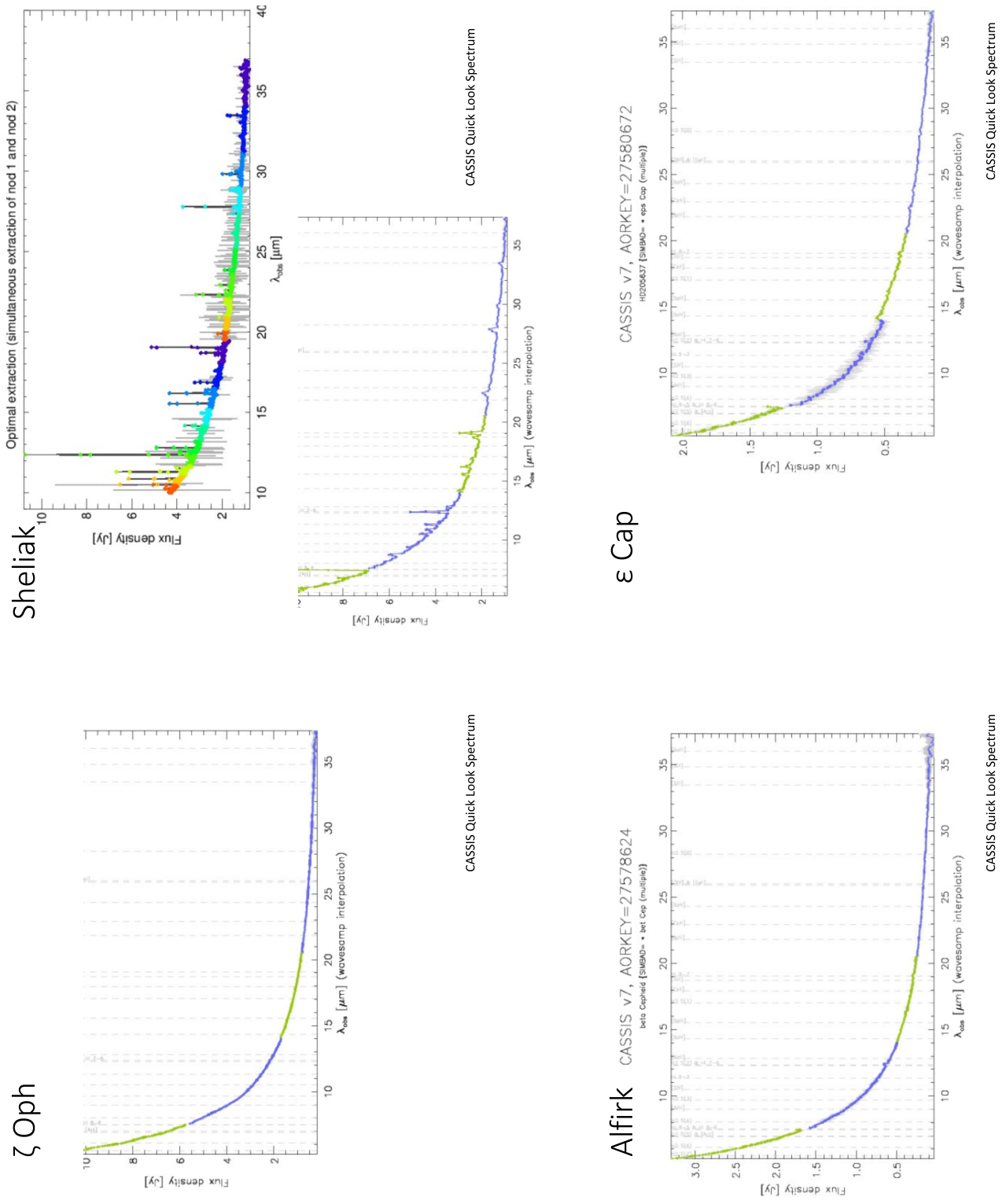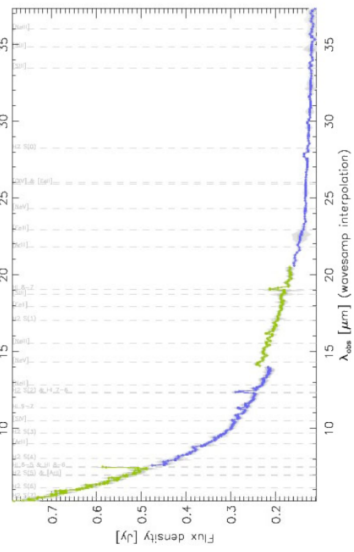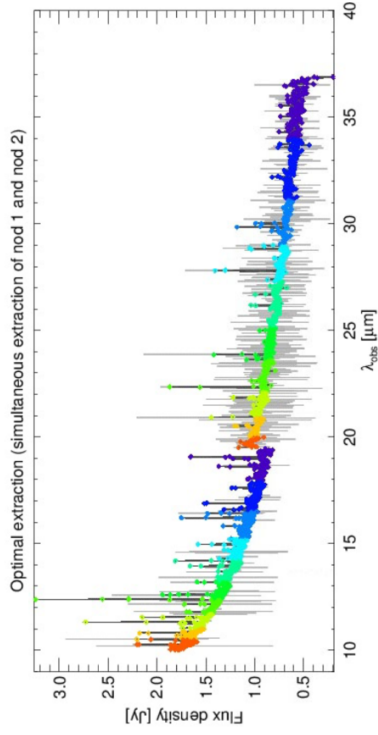
Figure 15: *Continued*

Figure 15: *Continued*

JAXA Research and Development Report   JAXA-RR-21-007E

SPICA Mid-infrared Instrument Calibration plan